UNIVERSITY OF OKLAHOMA

GRADUATE COLLEGE

IN VIVO FLUORESCENCE CHARACTERIZATION OF THE *ESCHERICHIA COLI* OUTER MEMBRANE PROTEIN FEPA

A DISSERTATION

SUBMITTED TO THE GRADUATE FACULTY

In partial fulfillment of the requirements for the

Degree of

DOCTOR OF PHILOSOPHY

By

CHUCK RANDALL SMALLWOOD
Norman, Oklahoma
2012

IN VIVO FLUORESCENCE CHARACTERIZATION OF THE *ESCHERICHIA COLI* OUTER MEMBRANE PROTEIN FEPA

A DISSERTATION APPROVED FOR THE
DEPARTMENT OF CHEMISTRY AND BIOCHEMISTRY

BY

_____
Dr. Ann H. West, Chair

_____
Dr. Phillip E. Klebba

_____
Dr. Elizabeth A. Karr

_____
Dr. Helen I. Zgurskaya

_____
Dr. Wai Tak Yip

_____
Dr. Shaorong Liu

This dissertation is dedicated to my wife, my parents, and my brother.

Acknowledgements

I want to first and foremost acknowledge my PhD advisor Dr. Phillip E. Klebba who readily provided training and supervision throughout my doctoral studies. Drs. Phillip Klebba and Sally Newton have encouraged and guided my scientific training, but also served as examples on how to balance everyday life with scientific research. My gratitude to them is unmatched and I truly appreciate the atmosphere and guidance they provided for my colleagues and myself. I had the great fortune of working with genuinely amazing people in the Klebba Lab and my exposure to those individuals has shaped who I am and who I will become.

I would like to express my sincere appreciation to all of my current and former committee members: Dr. Zgurskaya, Dr. Cook, Dr. Karr, Dr. Yip, Dr. West and Dr. Liu for their dedicated guidance and specialized course work that has given me insight to conduct proper scientific research. I would also like to acknowledge Dr. Ann West, who accepted the position of Committee Chair during my general exam and during my dissertation defense. Dr. West served as administrative advisor only and was not involved in the supervision of my dissertation research.

The work in this dissertation was built on the culmination of years of research from previous students to whom I offer my sincere gratitude. I owe special acknowledgements to Amparo Marco Gala, with whom I worked very closely during our first publication. I must express special thanks to Vy Trinh, a terrific scientist and excellent lab mate, whose dependability and genuine interest in her co-workers was always appreciated. My colleagues in Dr. Klebba's laboratory throughout the years are too many to list here, and although they have come and gone, the atmosphere in our group was always unique and I will forever treasure our shared experiences and disucussions.

"In scattering the seed, scattering your 'charity,' your kind deeds, you are giving away, in one form or another, part of your personality, and taking into yourself part of another; you are in mutual communion with one another, a little more attention and you will be rewarded with the knowledge of the most unexpected discoveries. You will come at last to look upon your work as a science; it will lay hold of all your life, and may fill up your whole life. On the other hand, all your thoughts, all the seeds scattered by you, perhaps forgotten by you, will grow up and take form. He who has received them from you will hand them on to another. And

how can you tell what part you may have in the future determination of the destinies of humanity?"

— Fyodor Dostoyevsky, The Idiot

Table of Contents

List of Tables

List of Figures

Abstract

Opportunistic microbial pathogens rely heavily on acquisition of nutrients to survive hostile environments. The complexity and redundancy of iron acquisition systems in bacteria illustrates the importance of iron in cellular processes. Siderophores are secreted into the extracellular environment to chelate iron, but these iron complexes must reenter through high affinity receptors, which belong to the ligand-gated porin (LGP) superfamily. The siderophore ferric enterobactin (FeEnt) is specific to the outer membrane (OM) receptor FepA, a 22-stranded β-barrel LGP that contains active surface loops and a N-terminal globular pore obstruction, that actively transports the ligand by unknown mechanism that is thought to require energy from the inner membrane (IM) TonB complex.

FeEnt binding is proposed to follow a two-state binding mechanism in the FepA surface loops where initial binding occurs in the individual loop extremities (B1) with subsequent collaboration of all surface loops and N-domain loops (B2) for uptake of the ligand through the FepA N-domain. We studied the reactivity of single Cys sites to fluoresceination that revealed thermal dependent loop conformational motion. Although toxins (ColB, ColD) bind to FepA receptor to enter and

kill the cell, results from the accessibility of multiple Cys sites to fluoresceination did not indicate that colicin B traversed the FepA channel to enter the cell, but may enter the periplasm through a different mechanism. Furthermore, the lack of TonB dependent labeling of multiple single Cys sites in FepA contradicted previous in vitro results of TonB-dependent loop conformation studies of both FepA and FhuA (1,2).

Studying the accessibility of multiple single Cys sites in the FepA surface loops provided an opportunity to analyze loop conformational motion with fluorescence spectroscopy in living cells. In vivo fluorescence changes of probes attached to individual FepA surface loops provided specific characterizations of loop motion during FeEnt uptake that quantified B1 and B2 rates of FeEnt binding in the loops. Furthermore, TonB-dependent loop conformational states revealed that differences in loop conformation exist during FeEnt uptake and a possible holding area for FeEnt exists, located between the interface of the FepA surface loops and N-terminal globular domain.

Chapter 1 : Introduction

Iron and Bacterial Pathogenesis

The discovery of antibiotics allowed human kind to overcome numerous attempted infections and illnesses by microbial pathogens, preventing and staving deaths for more than a century. As a consequence, our over prescribed use of antibiotics has allowed the ever adapting microbe to circumvent the actions of many of these once novel antimicrobial compounds resulting in broad resistance across genera (3). The current precedent of antibiotic resistance occurring around the world reveals the urgency for exploration of new methods of prevention and modes to fight pathogenic infections in humans (4).

Microbial pathogenesis within a human host stems from a microbe's innate ability to overcome environmental stress (i.e. immune system) that forces the organism to enact means of defense and offense in order to survive (5). The means of defense is multi-drug efflux pumps that have rapidly evolved to adapt over prescribed drugs (4). Iron acquisition is the common offense for many pathogens to incorporate iron into vital cellular process for their survival. Although iron is one of the most abundant metals in the earth's crust its low concentration in the extracellular environment due to iron insolubility (10^{-18} M) in the oxidizing

atmosphere limits its availability (6,7). Iron participates in many different vital cellular roles from oxidoreductive reactions in electron transport system (8) to the metabolic catalytic activity of aconitase that isomerizes citrate to isocitrate in the tricarboxylic acid cycle (9,10). These and other biochemical reactions require copious amounts of iron to perform vital cellular process. Thus, it is no surprise that opportunistic organisms have evolved a wide assortment of means to acquire iron from their surroundings (6,11).

Iron scavenging and siderophores

One mode of iron acquisition in bacteria is the production of low molecular weight iron scavenging molecules called siderophores (12,13). Siderophores are produced under iron deficient conditions (14). The regulator protein Fur (ferric uptake regulator) senses high iron concentration in the cell and acts as a negative regulator binding and inhibiting the promoter of genes that contribute to iron acquisition (15). The acidic low molecular weight (~670 Da) siderophore enterobactin (Ent) uses catecholate groups that bind iron with high affinity (Ka = 10^{52} M^{-1}), reducing Fe^{3+} to Fe^{2+}. This high affinity mechanism of enterobactin can even steal iron from other iron storage proteins such as transferrin in

extremely low concentration free-iron environments (16,17). Although ferric enterobactin (FeEnt) is relatively small, the siderophore is too large to diffuse through open pores in the OM of *E. coli,* requiring active transport across the membrane bilayer (7).

Metal ligand-gated porins

The uptake of metal ligands such as siderophores occurs through ligand-gated porins (LGPs), which bind metal ligands and transports them from the extracellular milieu to the periplasmic space. There are several different LGPs found in E. coli. The Gram (–) bacterium *E. coli* contains a cell envelope composed of two distinct layers, the OM and the inner membrane (IM), separated by the periplasmic space. The OM of Gram (–) bacteria provide protection against antagonistic molecules, but also regulate the entry of vital nutrients into the cell. High affinity binding and transport proteins are located in the OM and serve to selectively acquire nutrients vital to cellular function. Active transporters are gated for specific ligands, and are part of the LGP superfamily of transporters. Small molecules less than ~600Da can diffuse freely across the OM through open-channel porins (18). However, other molecules that are too large to diffuse through open porins, or are present at low concentration, require

energized transport by LGPs to cross the OM into the periplasmic space. Moreover, with the help of metal scavenger molecules (e.g. siderophores), metal-ligand receptors like FepA and other LGPs are able to acquire vital nutrients by actively transporting them into the cell against their concentration gradient (19,20). Although the transport mechanisms of these active transport OM proteins are still undetermined, some characteristics have emerged. For instance, the structural agreement and functional similarities between BtuB, FhuA, FecA, and FepA suggest a common mode of transport centered around the active participation of the receptor N-terminal domains and the inner membrane (IM) protein TonB (21). Moreover, with the help of metal scavenger molecules (e.g. siderophores), metal-ligand receptors like FepA and other LGPs are able to acquire vital nutrients by actively transporting them into the cell against their concentration gradient (19,20).

The active transport through LGPs, such as FepA, requires three important factors to transduce energy to these OM active transporters i) the proton motive force (pmf) from the cytoplasmic membrane (CM), ii) a cytoplasmic transmembrane complex composed of proteins TonB, ExbB, ExbD that spans the periplasmic space, and iii) a specific TonB-dependent transporter in the OM (21-24). TonB is thought to transduce

energy from the pmf of the CM providing a mechanical force to the active transporters that enables transport of nutrients across the OM (25). While this study does not address the potential mechanism of TonB function, we investigated the effect of TonB on conformational dynamics of FepA with fluorescence spectroscopy. Previous published data demonstrated that loop conformational motion of the transporter coincides with the presence of TonB (1,2). Moreover, the binding of the ligand to FepA proceeds in a biphasic reaction that first involves the initial binding of the ligand to the loop domain and then engulfing of the ligand by the loops in the receptor vestibule (26). It is unknown whether the FepA loops bind the ligand sequentially or simultaneously. Since binding still occurs in the absence of TonB, FepA loop conformational motions also appears to be dependent on the presence of the IM protein TonB (Fig.7) and were observed under both conditions.

The transmembrane pore of FepA is a 22-stranded β-barrel, which sits in the OM and surrounds a 150-residue globular N-domain. The internal residues of the β-barrel are postulated to stabilize the N-domain within the pore (27,28). The N-terminal domain composed of ~150 residues, forms a globular obstruction of four-stranded β-sheets connected by surface loops, turns, and short α-helices. The globular

structure of the FepA N-domain is similar to active transporters FhuA, BtuB, and FecA, whereas all of these receptors contain surface loops that bind specific metal-ligands and contain globular obstructions situated in their pores. The structures of these transporters initially seem very similar; however, a closer look reveals specific charged residues in the vestibule that distinguish each receptor and their affinity for specific ligands. For example, multiple arginine residues are located on the apical side of the FepA N-terminal globular domain, differentiating FepA from other OM active transporters (BtuB, FhuA, and FecA), which contain mainly aromatic residues at similar relative positions (29). These differences in the apical N-domain could hold a major significance in the binding mechanism of FepA to its ligand. The TonB box, a short conserved sequence near the N-terminus is postulated as the point of binding for the inner membrane (IM) protein complex TonB-ExbB-ExbD (30-33). In addition, evidence exists for conformational change in the loop domain of BtuB upon binding of the ligand, which alters the TonB coordination at the periplasmic interface (34). Fluorescence and surface plasmon resonance evidence revealed FhuA surface loops undergo conformational motion during formation of the TonB-FhuA complex (1). The structures of FhuA and FepA have structural homology in their N-

terminal globular domains, but no homology exists in the extracellular surface loop domains; both transport iron complexes through the OM of *E. coli*. Therefore, it is likely that FepA will also exhibit conformational motion similar to FhuA surface loops when TonB is present.

FeEnt binding and recognition in the FepA surface domain

Cao et al. (2003) conducted a spectroscopic analysis of four readily labeled Cys mutants, W101C, S271C, F329C, and S397C that reside on the cell surface-exposed loops of FepA above the LPS core sugars. Results showed changes in fluorescence intensity during active transport of FeEnt; these findings infer conformational motion of the FepA surface loops during ligand binding and transport, as fluorescence is quenched and subsequently restored after ligand uptake (35). Furthermore, specific conformational changes were seen in FepA loops L3 and L5 during ligand interaction, which suggests an open conformation in the absence of the ligand and a closed conformation upon binding of the ligand. In addition, when considered with the kinetics of biphasic binding of ligand adsorption to FepA, the data support a conformational change in FepA between open and closed states, which are likely similar in other LGPs: FecA, FhuA, and BtuB (26).

Cao et al. (2003) also investigated fluorescence quenching of S271C labeled with fluorescein-5-maleimide (FM) by the binding of different amounts of FeEnt (Fig. 1.1), demonstrating that binding remains functional despite the presence of a fluorescence label. Studies by alanine-scanning mutagenesis of acidic, basic, and aromatic residues on the surface domain of FepA revealed numerous contact points for the catechol groups of the acidic ligand FeEnt (29). Loop deletions were performed on 9 of the 11 active surface loops leading to three specific phenotypic results: slightly impaired (loops 3, 4, 5, 9), strongly impaired (loops 2, 10, 11), and abolished function (L7 or L8) (36). Loop deletions involve a large number of residues, a change that could compromise the over structure of the protein. However, even for single amino acid substitutions it is important to confirm that no major defects in FepA function result from the mutagenesis.

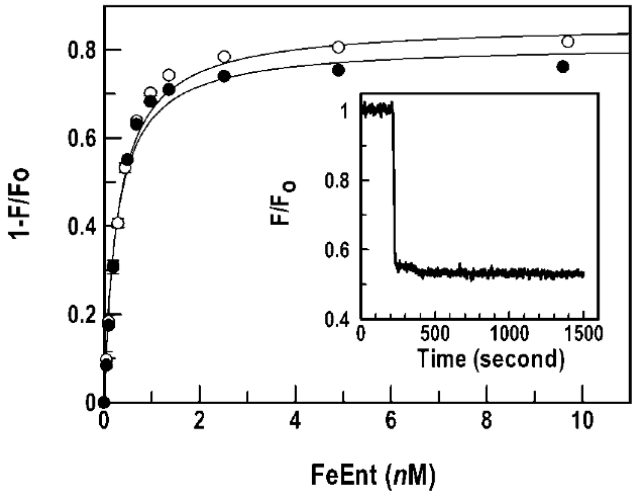

Figure 1.1 Cao et al. demonstrated FeEnt binding by fluorescein-labeled FepA.

S271C (open circle) & S397C (closed circle) were labeled with FM and diluted to 2.5 x 106/mL in TBS buffer, and fluorescence intensity was measured in the presence of varying amounts of FeEnt. Upon background and dilution correction, 1-F/F0 was fit against [FeEnt], using GraFit4 (Erithacus Software Ltd.) "Bound versus Total" equation. The Kd values for S271C and S397C were 0.263nM and 0.292nM, respectively. The inset shows the ability of FeEnt (added at 200 seconds) to quench the fluorescence of cells labeled with Alexafluor Maleimide in a comparable manner to ensure quenching of cells labeled with FM (35).

Possible Transport Models of FeEnt by FepA

The labeling of 25 different Cys mutation sites on FepA were conducted in the presence of FeEnt, which revealed strongly labeled residues in the surface loops of FepA, some labeling of N-terminal plug residues, no labeling of exterior and interior β-barrel residues, and poor labeling of N-terminal residues near the TonB box (37). The labeling of residue G54C during this study revealed a possible mechanism of transport for FepA. G54C, situated in the N-terminal globular plug, could be labeled in two ways: from the outside of the porin or from the periplasmic side. Labeling accessibility results indicated that the majority of G54C labeling by FM was from the periplasm (37). Interestingly, residues G565C, S569C, and T585C are all located on the interior β-barrel wall, in close proximity to G54C, but are not labeled by FM. These results were consistent with the idea that the N-terminal globular plug exits the β-barrel allowing FM to label G54C with greater intensity.

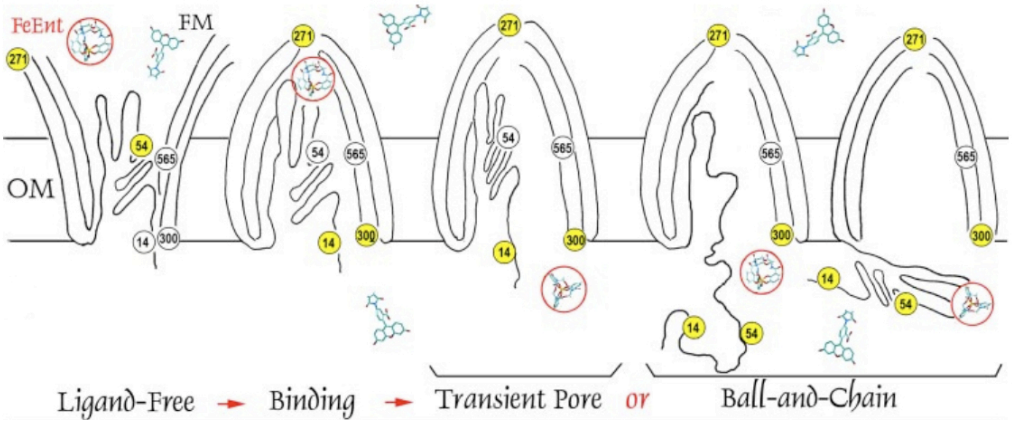

Figure 1.2 Ma et al. postulated FepA transport mechanisms.

The transient pore model stated that fluorophores must enter FepA to react with the N-terminal domain; whereas the ball-and-chain hypothesis stated that fluorophores labeled the N-terminal domain while in the periplasm when either portions or the complete domain dislodged from the β-barrel [figure adapted from (37)].

The labeling results of G54C (37) and other residues located inside the barrel of FepA led Ma et al. to discriminate between the Transient Pore and Ball-and-Chain model (Fig. 1.2), which suggested that the labeling of multiple cysteine sites in FepA in the absence and presence of FeEnt supported the ball-and-chain hypothesis (37). The ball-and-chain hypothesis predicted that the N-terminal globular domain exits the β-Barrel either partially or completely. Recent work provided further insight into the conformational dynamics of FepA siderophore binding, which indicated that the surface loops of FepA participate in concerted motion during the uptake of FeEnt (31,36-40). Although, these recent studies did not investigate the action of the N-terminal domain, these results from global accessibility of FM in FepA under different conditions and FepA loop conformational motion could be used to elucidate a possible binding and transport mechanism.

Research carried out in this dissertation

Previous constructs developed by Ma et al. (37) were used and additional single Cys site mutants were engineered with a total of 35 Cys sites in FepA, which were labeled with the fluorophore fluorescein-5-

maleimide (FM) under various conditions. Smallwood et al. (40) utilized the accessibility of FM to various Cys mutation sites within FepA to explore the conformational dynamics of surface loops under different conditions of temperature and presence or absence of a ligand (the protein toxin Colicin B, ColB). The accessibility of FM to strategic engineered Cys sites revealed further information on the structural states of the FepA loops. Results obtained at different thermal states during FepA interaction with ColB revealed patterns of conformational changes consistent with open and closed conformation states that were independent of TonB (40). The presence of ColB led to little or no FM-labeling of loop residues, while intense labeling occurred in the absence of ColB. From the FM-labeling data, we concluded that the globular domain does not exit the barrel when ColB was present. However, fluorophore labeling at different temperatures (Fig. 3.6) did confirm loop motion (1,31,41). Results from temperature studies indicated conformational changes occur in the FepA loops upon thermal transition from the closed form at low temperature, to the open form at higher temperatures (Fig. 3.6). For example, when the temperature increased from 0°C to 37°C, fluorophore labeling of residues increased 2- to 3-fold (residues 101, 216, 271, 383, 698) and 7- to 10-fold (residues 63, 322, 470, 482, 550). This

suggested dynamic motion was occurring in the loops of FepA during the temperature transition.

Fluor accessibility studies (37,40) characterized multiple sites in FepA that provided insight into possible binding and transport models. In addition, Ma et al. (37) results from *in vitro* and *in vivo* characterization of FepA binding and transport provided general mechanistic trends of the reactivity of FepA to its ligand that were biologically relevant. Furthermore, fluorophore accessibility studies served as a guide for the investigation into conformational dynamics of the surface loop conformational motion using fluorescence spectroscopic studies of FM-labeled residues during FeEnt binding and transport. Characterizing the motion of each individual loop refined previously published data that estimated a 15 Å range of loop motion (31,42). Fluorescence spectroscopy and surface plasmon resonance evidence revealed FhuA surface loops undergo conformational motion during formation of the TonB-FhuA complex (1). FhuA and FepA are very similar in structure and both transport iron complexes into the cell. Therefore, due to their similarities it was likely that FepA would exhibit similar conformational motion to FhuA in the surface loops when TonB is present. Thus, these studies provided additional evidence of the dynamic binding mechanism and transport mechanism of FepA.

Chapter 2 : General materials and methods

Bacterial strains, plasmids and culture conditions

Bacterial strains (37)OKN1 (Δ*tonB*), OKN3 (Δ*fepA*), and OKN13 (Δ*tonB*, Δ*fepA*) harbored the low-copy plasmids pITS23 (31) or pITS47, which carry *fepA*$^{+}$ or mutant *fepA* alleles under control of their natural Fur promoter (Table 2.1, host strains; Table 2.2, plasmid vectors). Existing Cys substitution mutations were carried on pITS23 (37); new constructions were on pITS47, which is identical to pITS23 except that it was generated with difference restriction sites flanking the *fepA*$^{+}$ gene. pITS47, we amplified *fepA*$^{+}$ and its upstream promoter region from *E. coli* chromosomal DNA, flanked by Pst1 and HindIII sites, and cloned it into Pst1 and HindIII-cut pHSG575 DNA (43,44).

Table 2.1 Host strains

Host Strain	Relevant genotype or gene	Reference or source
BN1071	*F- thi entA fepA $^{+}$pro trpB1 tonB^{+}rpsL*	Klebba 1982(43,45)
KDF541	*F- leu pro trp thi rpsL recA entA fepA^{-} fhuA^{-} cir^{-}*	Rutz 1992 (*45*)
KDF571	KDF541 *tonB^{-}*	Rutz 1992 (46)
OKN3	BN1071 *fepA^{-}*	Ma 2007 (37)
OKN1	BN1071 *tonB^{-}*	Ma 2007 (37)
OKN13	BN1071 *fepA^{-} tonB^{-}*	Ma 2007(37)
T184	lacY^{-} z^{-}	Teather 1980(47)

Table 2.2 Plasmids / vectors

Plasmid(s)	Relevant genotype or gene	Reference or source
pHSG575		Hashimoto-Gotoh 1981(43)
pUC18	high copy vector	Yanisch-perron 1985(48)
pits23	pHSG575fepA (full promoter)	Ma 2007 (37)
pits449	pUC18 fepA (high copy)	Annamalai 2004(49)
pits47	fepA	Smallwood 2009(50)
pLacY	lacY lac promotor	
pLp271	lacY-GFP (pt75), fepA(pits23-S271C)	this study
pGT	pHSG575 *tonB promoter-ssgfp*(GFP-TonB)	Kaserer 2008 (51)
pGT/271	pGT and pits449 S271C	this study
pTpG	pHSG575 tonB promoter:ssgfp(GFP)	Kaserer 2008 (51)
pCol1	pUC18 cba cbi (colicin B)	Kaserer 2008 (51)
pHis6FepA	pits47 N-term 6-histag FepA	Dr. Kyle Moore (this study)

Culture conditions consisted of an initial inoculation into LB media and subculture into MOPS minimal media, an iron deficient medium(52). Concentrations of appropriate antibiotics in medium were 100μg/mL Streptomycin, 20μg/mL Chloremphenicol and 100μg/mL Ampicillin unless stated otherwise. The carbon source for all fluorescence studies was 0.4% glucose, which was also added to all buffers used during fluorophore modification of Cys sulfhydryl groups. For strains containing *lacZ* promotor

1mM of IPTG was added to cultures in mid log phase of growth. Reducing agents used were 1mM of cysteine, 2-mercaptoethanol (SIGMA).

For loop conformational motion study we developed additional constructs similar to the fluor accessibility study. Host strains were OKN3 (BN1071 *fepA*$^{-}$) or OKN13 (BN1071 *fepA*$^{-}$ *tonB*$^{-}$*)* containing plasmids pits23 (37) or pits47 (40) with Cys mutations in the *fepA* gene. Dr. Kyle J. Moore designed 6-histag on the N-terminus of FepA to easily purify FepA protein for western blot expression analysis. All bacteria were grown in 37ºC shaking incubator overnight in Luria–Bertani (LB) broth (53) with streptomycin (100 μg/mL) and chloramphenicol (20 μg/mL). Strains were then sub–cultured (1%) into iron deficient conditions of MOPS minimal media or T–media containing the aforementioned antibiotics for biochemical and live cell fluorescence spectroscopic experiments. Cultures were harvested after 5.5 hours of growth in minimal media and prepared for fluor labeling.

We purified enterobactin from large growth cultures of T-media (54,55). Forming complexes of enterobactin with $FeSO_4$ before each experiment ensured minimal amounts of oxidized iron complexes throughout this study. These complexes were verified using UV/Vis spectroscopy and the concentration of the siderophores were measured

from the absorbance at 495 nm. All spectroscopic and radioisotopic experiments were conducted with fresh FeEnt that was less than two weeks old.

Single cysteine site-directed mutagenesis

We used QuikChange mutagenesis (Stratagene, San Diego, CA) to create mutations in *fepA* on pITS47 that encoded Cys substitutions at A12, N39, A42, T51, N56, A59, S63, G76, W101, G127, and N135. We also used KAPA mutagenesis (Kapa Biosystems Inc., USA) to create mutations in in *fepA* on pITS47 that encoded Cys substitutions at A261, S275, G327, G640, T648, and S490. After verification by DNA sequence analysis (McLab, San Francisco, CA) we evaluated the colicin B and D sensitivity, ability to transport FeEnt, and expression levels of the mutant FepA proteins (Newton et al., 1999): except for W101C all phenotypes were indistinguishable from wild-type FepA.

Table 2.3 FepA single cysteine mutations

FepA Cys Mutation[a]	FepA Domain	Reference / Source
D11C[b]	N-domain	unpublished
D12C[b]	N-domain	Smallwood et al. (40)

I14C	N-domain	Ma et al.(37)
V16C[b]	N-domain	unpublished
A33C	N-domain	Ma et al.(37)
T32C[b]	N-domain	unpublished
D34C[b]	N-domain	unpublished
N39C[b]	N-domain	Smallwood et al. (40)
A42C[b]	N-domain	Smallwood et al. (40)
T51C[b]	N-domain	Smallwood et al. (40)
G54C	N-domain	Ma et al. (37)
N56C[b]	N-domain	Smallwood et al. (40)
G59C[b]	N-domain	Smallwood et al. (40)
S63C[b]	N-domain	Smallwood et al. (40)
S92C	N-domain	Ma et al. (37)
W101C[b]	N-domain	Smallwood et al. (40)
T107C	N-domain	Ma et al. (37)
G127C[b]	N-domain	Smallwood et al. (40)
N135C[b]	N-domain	Smallwood et al. (40)
T216C	L2	Ma et al. (37)
S254C	β-barrel	Ma et al. (37)
A261C	β-barrel / L3	Ma et al. (37)
S271C	L3	Ma et al. (37)
S275C[b]	L3	Vy Trinh (this study)
G300C	β-barrel	Ma et al. (37)
A322C	L4	Ma et al. (37)
G327C[b]	L4	this study
T367C	β-barrel	Ma et al. (37)
A383C	L5	Ma et al. (37)
S411C	β-barrel	Ma et al. (37)
S470C	L7	Ma et al. (37)

S482C	L7	Ma et al. (37)
S490C	L7	Jessica Jensen (this study)
S507C	β-barrel	Ma et al. (37)
T550C	L8	Ma et al. (37)
G565C	β-barrel	Ma et al. (37)
S569C	β-barrel	Ma et al. (37)
T585C	β-barrel	Ma et al. (37)
S600C	β-barrel / L9	Ma et al. (37)
T609C	β-barrel	Ma et al. (37)
G640C[b]	L10	this study
T648C[b]	L10	this study
T666C	β-barrel	Ma et al. (37)
A698C	L11	Ma et al. (37)

a. In OKN3 (fepA, tonB$^+$) the native fepA$^+$ promoter on pITS23 conferred wild-type expression levels for all mutant proteins. Upon verification by DNA sequencing we evaluated colicin B sensitivity, ability to transport FeEnt, and expression of the mutant FepA proteins to ensure their phenotypes were identical to wild type.

b. Single cysteine mutations that were designed in pITS47

For the study of FepA loop conformational motion we selected mutants based on the fluor accessibility results on the surface of FepA that display high FM accessibility to Cys sites. We designed additional FepA surface loop Cys sites (S275C, G327C, S490C, G640C, and T648C) with the Qiagen mutagenesis kit (Qiagen; San Francisco, CA). All sulfhydryl sites on the surface loop sites are highly accessible to fluorophore modification. These Cys mutants were designed in accordance with numerous aromatic and basic residues that were

identified to possibly contribute to the binding and uptake of FeEnt (26,49). Phenotypes of our mutants were measured using siderophore nutrition assay and colicin killing assay for qualitative uptake of iron and susceptibility to the bacteriocin Colicin B (ColB), respectively.

FeEnt, ColB and FepA

We formed and purified FeEnt (49) and determined its concentration from the extinction coefficient (5.6 mM^{-1}) at 495 nm. We purified colicin B from cultures of *E. coli* strain DM1187/pCLB1 (26) and determined the stoichiometry of the FepA–ColB interaction as follows: FepA is present in BN1071 at 37.3 pmol per 10^9 cells (51), and for labeling reactions with ColB we diluted 20μL of purified toxin (0.8 mg mL^{-1}) into 1 mL containing 5 x 10^8cells, resulting in final concentrations of 0.28 μM ColB and 0.019 μM FepA (i.e. 15 fold excess ColB). The K_d of the ColB–FepA binding interaction is 0.185 μM (26) so at binding equilibrium FepA was 49% saturated with ColB. Microbiological plate counts after labeling reactions in the presence of ColB showed that this protocol resulted in 99.85% mortality of the bacterial cells.

Siderophore nutrition assay

The strain of interest was grown in LB media to OD600 late log phase. Warmed Tryptone or Nutrient Top Agar was incubated in a water bath at 50ºC. Tubes were prepared with 100uL of bacterial culture and appropriate antibiotics for the strain of interest, and 7uL of 0.1 M bipyridyl and 3mL of Top Agar was added to the tubes, gently vortex, placed in well of a 6 well plate and allowed to solidify. Once solid, a blank paper disc (Becton, Dickinson and Company, France) was positioned in the center and 0.5 nmol of iron siderophore was placed on the disc. Plates were allowed to incubate at 37ºC overnight and the diameter of growth surrounding each disc was measured.

FepA purification by ColB-Sepharose column chromatography

Aliquots of Sepharose 6B were activated by the drop wise addition of 4g of CNBr in 4mL of DMF with gentle mixing for 6 minutes, and maintaining the pH at 11 until equilibrium is achieved (56). The resin was rinsed with distilled water and resuspended in cold 0.2 M $NaHCO_3$ buffer. Dialyzed colicin B was mixed with resin slurry and allowed to conjugate overnight. The ColB-Sepharose was cold rinsed in sequential order with

equal volumes of distilled water, 1 M acetic acid, distilled water and finally 1x MOPS 1% NaCl for storage at 4ºC.

For purification of FepA from cell lysate, 50mM Tris at pH 7.2 containing 2% Triton X-100, 5mM EDTA and 0.1% NaN_3 was added to the activated resin, and incubated overnight at 4ºC (57-59). BN1071 cells with desired plasmid containing FepA were grown overnight in 5mL of LB from frozen stock and then subculture to 150mL of LB and allowed to grow for 10 hours. The entire culture was subculture in 15 liters of T-media at 37ºC with aeration until OD600 reached late log (54,55). Cells were harvested by centrifugation and washed with 10mM Tris, 10mM benzamidine pH 8.0, resuspended in 10mM Tris. The process was repeated then the cells were lysed using French Pressure Cell Press (SLM Aminco). The lysed cells were centrifuged at 3000 rpm for 10min to separate unlysed cells. The cell lyses supernatant was ultracentrifugated at 30,000 rpm for 40 minutes to pellet membranes. Membranes were washed twice with 50mL of 10mM Tris at pH 8.0, 10mM $MgCl_2$, 10mM benzamidine and centrifuged for 40 minutes at 30,000 rpm. Cell lysates were resuspended in 50mL of 2% Triton X-100, 100mM Tris, 10mM benzamidine and shaken at room temperature for 30 minutes. Insolubilized membranes were pelleted by centrifugation and the

supernatant that contained cytoplasmic membranes was discarded. After a repeat of the extraction of cytoplasmic membranes the pellets were washed with 50mL of 10mM Tris at pH 8.0, 10mM benzadine and pelleted for 40 minutes at 30,000 rpm. The pellets were resuspended in 50mL of 2% Triton X-100, 10mM Tris at pH 8.0, 5mM EDTA, 10mM benzamidine, and shaken for 30 minutes. These murein fractions were again pelleted by ultracentrifugation and the extraction was repeated, and the final pellets were discarded. The solubilized outer membrane proteins were dialyzed in 4 L of 50mM Tris at pH 7.2, 2% Triton X-100, 5mM EDTA (TTE) and loaded onto the ColB-Sepharose affinity column. The ColB-Sepharose column was washed with 10 column volumes of TTE and the solubilized outer membrane proteins were introduced and eluted with a 1 to 2.5 M NaCl gradient in 0.2% TTE. Fractions were analyzed by SDS-PAGE and Lowry method was used to determine FepA protein concentration.

Histag-FepA purification by Ni-NTA chromatography

The procedure for histag-FepA involved the same steps for solubilizing the outer membrane proteins from the cell lysates. The solubilized other membrane proteins were twice dialyzed in TTN (no EDTA) to remove all traces of EDTA that could affect the Ni-NTA column

(QIAGEN Sciences, USA). The column was prepared by equilibrating 5mL Ni-NTA resin in TTN and rinsing with 10 column volumes of TTN. The histag purification procedure from QIAGEN was used to purify the histag-FepA. Fractions were analyzed by SDS-PAGE and Lowry method was used to determine FepA protein concentration. Histag-FepA was used as a standard to determine amount of FepA present in western blot.

Bacteriocin colicin B killing assay

The strain of interest was grown in LB media to OD600 late log phase. Warmed LB Top Agar was incubated in a water bath at 50ºC. Tubes were prepared with 100μL of bacterial culture and appropriate antibiotics for the strain of interest; 3mL of Top Agar was added to the tubes, gently vortex, plated as a lawn on LB Agar plate. A micro titer master plate was prepared using a sample of ColB with high measurable activity and concentration. Dilutions of the ColB in the master plate were prepared starting in the far upper left well with a 1:10 down vertically and 1:2 horizontal dilutions in 100μL columns. A Mastercloner™ was dipped in the master plate wells and carefully placed on the prepared bacterial lawn of the LB plate. The plates were then incubated at 37ºC overnight and the colicin B killing strength of titer was measured visually.

Kinetics of colicin B killing

ColB kills bacterial cells by insertion of its C-terminal pore-forming domain into the IM. We utilized the fluorescence emissions of 3, 3'-diethyloxacarbocyanine ($DiOC_2(3)$; (60), which reflects cellular membrane potential, to observe ColB-induced depolarization. BN1071 (*fepA*$^+$, *tonB*$^+$) and OKN13 (*ΔfepA, ΔtonB*) were grown overnight in Luria–Bertani broth, subculture (1%) into MOPS minimal media with glucose and nutritional supplements, and grown to late-log phase ($OD_{600} \approx 0.9$). The bacteria were pelleted by centrifugation, resuspended in PBS plus 0.4% glucose at 5×10^8 mL^{-1}, and exposed to purified ColB for varying times (5–30 min). $DiOC_2(3)$ was added to 3 μM, incubated 30 min at room temperature, and the cells were immediately analyzed on a Beckman-Coulter Epics Elite flow cytometer at 575 nm. Emission data were collected with log amplification and mean red fluorescence intensity was plotted versus time. The results were compared with those from bacteria, which were not exposed to the bacteriocin, and to the same strains exposed to the bacteriocin, and to the same strains exposed to 5 μM carbonyl cyanide 3-chlorophenylhydrazone.

Fluorescence labeling of FepA Cys sites in vivo

We fluoresceinated Cys sulfhydryl residues in FepA in live cells (37). After growth in MOPS media to mid-log phase (4–5 x 10^8 cells mL^{-1}; 5–6 hr), we collected the bacteria by centrifugation, and washed and resuspended them in 50 mM $NaHPO_4$, pH 6.5. To equilibrate cells, the samples were pre-incubated in a 37ºC water bath for 10 mins. F5M or A488M (Invitrogen) was added to the cells at 5μM for 15 min, at 0ºC or 37ºC, the reactions were quenched with 100μM cysteine, and the cells were washed with and resuspended in ice-cold TBS. After determining cell concentration by absorption at 600 nm, we lysed 10^8 bacteria by boiling in SDS-PAGE sample buffer, and subjected the lysate to SDS-PAGE, which verifies proper folding of FepA with mutation.

Detection of labeling: SDS-PAGE, fluorescence imagery and immunoblots

Bacterial cell proteins were subjected to SDS–PAGE (36,61), rinsed with water and imaged with a STORMSCAN fluorescence imager (GE Life Science, USA). Proteins were transferred to nitrocellulose from gels and developed with mouse anti-FepA mAb 41/45 (0.5%; (62)) and ^{125}I-protein A (36). Upon exposure of ^{125}I-protein A blots to

phosphoimaging screen, we measured radioactivity on the STORMSCAN phosphoimager (GE Life Science, USA).

Image analysis

Scanned images of SDS-PAGE fluorescence and [^{125}I] emissions were analyzed by ImageQuant 5.2 (Molecular Dynamics). For relative measurements of FepA fluorescence we determined the intensity of the FepA band in each lane of the gel, relative to the fluorescence of a cellular protein that was labeled at constant levels (Band 3; (37)). Absolute measurements of FepA fluorescence were determined by running aliquots of purified FepA in gels, and used them as standards in the [^{125}I]-protein An immunoblots to determine the precise quantity (μg) of FepA in each lane. From these data we calculated the fluorescence intensity of the FepA bands per μg FepA protein.

Fluorescence spectrophotometry

All fluorescence spectroscopic measurements were performed using the SLM 8000 fluorospectrophotometer upgraded to SLM 8100 (Aminco, USA). Fluorescently labeled cells were prepared as previously described by Cao et al. (2002) and resuspended to 5x10^{8} cells in 1mL

MOPS with 4% glucose. We recorded fluorescence time course studies of $2.5x10^7$ cells in 2mL MOPS, 4% glucose with moderate mixing at room temperature(35). The excitation and emission wavelengths were 490nm and 518nm for both F5M and A488M labeled cells. All slits on the SLM were set at 16mm for measurements in this study. Freshly purified FeEnt was introduced at indicated concentrations after stable fluorescence levels were collected and the fluorescence intensity change was monitored over time. Fluorescence spectroscopic data was aligned for insertion of the ligand FeEnt and analyzed in GraFit 7.0

Siderophore binding assay

The radioactive siderophore binding reaction was modified version from previous studies conducted completely on ice(36). Bacterial strains of interest were grown overnight at 37ºC in LB broth then subculture in MOPS minimal media and allowed to grow to late log (~5.5 hours) cells were isolated and treated with fluorophores as previously indicated or unlabeled and resuspended in a 2mL at $5x10^8$ cells per mL and placed on ice for at least 10 minutes. The radioactive ^{59}FeEnt was prepared with a specific activity ~150-400 cpm/pmol and purified chromatographically. All binding reactions were done on ice at 0ºC in triplicate at 59FeEnt

concentrations of 0.05, 0.1, 0.5, 1.0, 5.0, and 10.0 nM. Each concentration of radioactive siderophore was incubated on ice with the cells for 5 seconds in 10mL of ice cold MOPS, 0.4% glucose then filtered mixture through 0.45 micron PROTRAN BA 85 nitrocellulose filters (Whatman, Germany) and rinsed with 10mL of ice cold 0.9% LiCl chaotropic agent. The radioactively (cpm) of the bound cells was counted using a gamma counter and analyzed according to the measured specific activity of the 59FeEnt. The Kd and capacity of binding for the tested strains were measured by plotting pmol of FeEnt per 10^9 cells versus concentration of ^{59}FeEnt. Samples were saved and tested for presence of fluorophore and FepA protein expression.

Siderophore transport assay

The functionality of the fluorophore-modified strains were questioned and we tested them using the radioactive ^{59}FeEnt transport assay. Bacterial strains of interest were grown overnight at 37ºC in LB broth then subculture in MOPS minimal media and allowed to grow to late log (~5.5 hours) cells were isolated and treated with fluorophores as previously indicated or unlabeled and resuspended in a 1mL at $5x10^8$ cells per mL. The radioactive ^{59}FeEnt was prepared with a specific activity

~150-400 cpm/pmol and purified chromatographically by Dr. Klebba. All transport reactions were conducted with 25 nM 59FeEnt at 37ºC for two different periods of incubation, 5 seconds and 1 minute. The cells were then filtered through 0.45 micron PROTRAN BA 85 nitrocellulose filters (Whatman, Germany) and rinsed with 10mL of 0.9% LiCl chaotropic agent. The radioactively bound cells were counted using a gamma counter and analyzed according to the measured specific activity of the ^{59}FeEnt. The difference of the counts from the two different time periods were calculated, which allowed the determination of Km and Vmax for transport by plotting pmol of FeEnt per 10^9 cells per minute versus concentration of ^{59}FeEnt in GraFit 6 (Erithracus Software). Samples were saved and tested for presence of fluorophore and FepA protein expression.

Confocal microscopy sample preparation

Bacterial cells from frozen stocks were grown overnight in 5mL LB broth cultures. Cells were subculture into MOPS minimal media and allowed to grow for 5.5 hours. Strains that needed to be induced were subculture into MOPS minimal for 2 hours then induced with 1mM IPTG and allowed to grow for another 2 hours. From the measured OD_{600} $5x10^8$ cells/mL were centrifuged and resuspended in 1mL of ice cold labeling

buffer and kept on ice in preparation for fluorophore modification as previously described. Glass slips were treated with poly-lysine solution and allowed to dry. For confocal sample preparation 10uL of $5x10^8$ cells/mL was placed on a glass microscope slide, the poly-lysine coated cover slip was placed on the cells for 5 minutes to allow the poly-lysine to fix the *E. coli* cells to the glass to prevent their motility during imaging. Cells were imaged with Olympus FV1000 Confocal/MP microscope with a 100x/1.42NA objective.

In vivo fluorescence labeling and characterization by fluorescence spectroscopy

To characterize FepA surface loop motion we used fluorescence spectroscopy as performed previously in Cao et al. and other studies from our lab. Strains were grown in MOPS minimal media until late log (OD600=0.9), $5x10^8$ cells were pelleted and resuspended in 1mL of labeling buffer (50mM Na_2HPO_4, 0.9% NaCl, 0.4% glucose pH 6.5). Cell suspensions were washed with labeling buffer and preincubate at 37ºC for 10 minutes prior to fluor labeling. Cells were incubated for 15 minutes at 37ºC with 5uM Fluorescein-5-Malemide (FM) or AlexaFluor® Maleimide 488 (AM488) (Life Technologies; Grand Island, NY) in DMSO. The

labeling reaction was then quenched with excess Cysteine, washed with labeling buffer and resuspended in 1x MOPS buffer with 0.4% glucose. Spectroscopic time course observations of the FM–labeled cells were performed in the upgraded SLM AMINCO 8100 fluorescence spectrophotometer at 25ºC. Fluorescence time course studies were conducted with $2.5x10^7$ cells/mL of labeled cells in 2mL of 1xMOPS buffer with 0.4% glucose in quartz cuvettes, and FeEnt was introduced at concentrations for indicated time points. The data collected from fluorescence time courses were aligned by FeEnt insertion, analyzed and fitted with GraFit 6.0.1 Data Analysis Software (Erithacus Software Ltd.).

Fluorescence quenching and recovery rate analysis

Fluorescence quenching from the normalized time course data were subjected to a double exponential decay equation with offset ($A(t) = A_{0(1)}e^{-k1t} + A_{0(2)}e^{-k2t}$ + offset) resulting in two rate constants k1 and k2, which were used to calculate the half-life decay rates for binding state B1 and B2, respectively. Fluorescence recovery curves were inverted by subjecting the data to –LOG(F/F0) and fitted with a single exponential decay equation with offset ($A(t) = A_0e^{-kt}$ + offset), which were used to

calculate the half-life recovery times for each individual FM-labeled loop. Data were analyzed in GraFit 6.0.1.

Radioisotopic binding and transport assay

59FeEnt biochemical binding and transport measurements characterized the effects of covalent modification of Cys residues and FM-label in the FepA surface loops in living cells. We purified the sidereophore enterobactin (Ent) then formed complexes with ^{59}Fe. Cells were isolated and subjected to the fluorescence labeling protocol with or without the fluorophore to maintain constant treatment of unlabeled versus labeled cells. Cells were resuspended in MOPS buffer with 0.4% glucose and kept on ice during binding experiment. We determined the Kd and capacity of ^{59}FeEnt binding using the bound-versus-total equation of GraFit 6.0.1. The transport function of each mutation, with and without the presence of the fluor label, were performed at 37ºC and allowed to incubate with concentrations of the siderophore for periods of 5 seconds and 65 seconds. The Km and Vmax for each sample were calculated from the amount of ^{59}FeEnt transported in 60 seconds using the enzyme kinetics equation in GraFit 6.0.1 analysis software.

Chapter 3 : Fluoresceination of FepA during colicin B killing: effects of temperature, toxin and TonB.

Background

The natural function of the *Escherichia coli* outer membrane (OM) protein FepA is recognition and uptake of ferric enterobactin (FeEnt) ((63); (64); (65)). Bacteriocins [in the case of FepA, colicins B (colB) and D (66); (39)] and viruses [bacteriophage H8 (32)] parasitize bacterial solute and nutrilite uptake pathways. Colicins initially interact with an OM receptor protein, denature and unfold on the cell surface (67) (68), and then transfer a functional domain that kills the cell by mechanisms like inner membrane (IM) depolarization or degradation of nucleic acids or peptidoglycan. One model of colicin uptake through the OM involves movement of the toxin polypeptide through a transmembrane porin channel (68,69). FepA and its homologues contain a C-terminal, 22-stranded porin channel (70) and a globular N-terminus (N-domain) inside the pore. Without structural rearrangement, the N-domain in the channel prohibits the passage of a metal chelate or a bacteriocin. This enigma may be resolved by conformational motion that forms a transient pore or moves the N-domain out of the channel (2,37,71). The energetics of

colicin uptake is not definitively known, but colicin activity requires the additional cell envelope proteins TonB (72-75) or TolA (76,77). TonB-dependent metal transport, and Tol-dependent cellular systems are energy dependent (78-81). These requirements are not fully understood: the OM cannot sustain an ion gradient because of its open channels (82); TonB and TolA are minor cell envelope proteins whose exact functions are unknown. The N-termini of both proteins are postulated to reside in the IM, but their C-termini interact with OM proteins (83-85), suggesting that they span the periplasm. Consistent with this idea, the TonB C-terminus also binds peptidoglycan (51), and the C-terminus of TolA binds the peptidoglycan-associated protein Pal (86). The requirements for energy and TonB during FepA-mediated transport may relate to the structural rearrangement of the receptor protein's globular N-domain, noted above. Ligands bind to FepA in biphasic reactions (26). FeEnt first adsorbs to residues in the loop extremities (29,49), and loops ultimately coalesce around it (27,31), ensconcing the metal complex in the receptor's vestibule at binding equilibrium. Ligand binding generally elicits structural changes in the N-domain that relocate the TonB-box away from the b-barrel wall, signaling receptor occupancy at the periplasmic side of the OM (87,88). However, this phenomenon does not occur during binding of ColIa to Cir

(89) *in vitro*. These initial stages of ligand uptake occur with equivalent affinity and rate in energy-sufficient or -deficient, and *tonB* + or *tonB* cells (35,36). In *tonB* +, *fepA* + cells the C-terminal domain of ColB causes cell death by forming a depolarizing channel in the IM. *tonB* cells survive ColB, presumably because its killing domain does not penetrate their OM. To assess models of ColB transport we studied the accessibility of genetically engineered Cys side-chains in FepA to covalent modification by fluorescein maleimide (FM). The reagent strongly labeled surface loop sites. These reactions were temperature-dependent, and inhibited by ColB binding to FepA. However, we did not observe increases in the accessibility of any Cys residues in FepA during ColB killing at 37°C. Thus, we found no evidence that the ColB polypeptide passes through the FepA channel.

Results

Kinetics of ColB binding and killing

We used the membrane soluble carbocyanine dye DiOC2(3) to cytometrically measure the time required for ColB-induced depolarization of *E. coli* cells. DiOC2(3) associates with and accumulates in bacterial cells; changes in its emission spectrum reflect alterations in cell

membrane potential (90,91). Upon exposure of the ColB-sensitive strain BN1071 (*fepA* +, *tonB* +) to ColB and DiOC2(3), cell-associated red fluorescence increased within 5 min and reached maximum levels by 30–40 min (Fig. 3.1). Conversely, red fluorescence of the ColB-resistant strain OKN13 (*fepA*, *tonB*) did not increase during incubation with ColB and DiOC2(3), whereas the control depolarizing agent carbonyl cyanide 3-chlorophenylhydrazone increased the fluorescence of both BN1071 and OKN13. On the basis of these and other findings (67,92), we exposed the bacteria to excess ColB (0.28 mM; 15-fold molar excess over [FepA]; see *Experimental procedures*) for 30 min at 0°C or 37°C prior to the initiation of FM labeling, which was 15 min in duration.

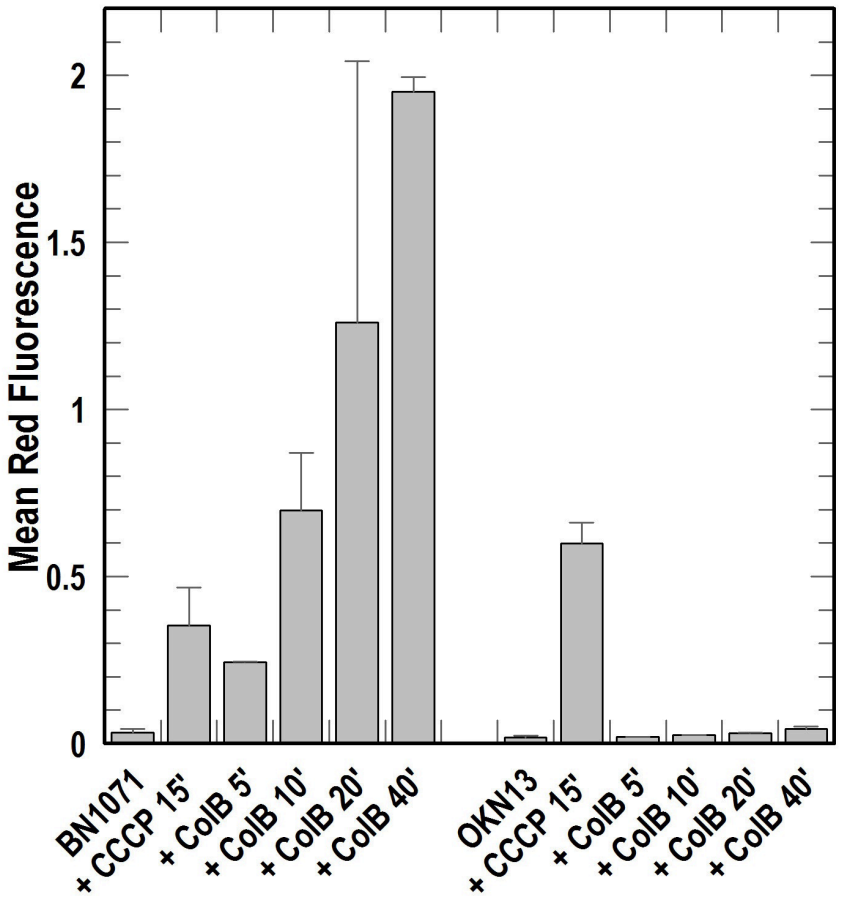

Figure 3.1 Kinetics of ColB–mediated lethality.

E. coli strains BN1071 (*fepA*$^{+}$*, tonB*$^{+}$) and OKN13 (*fepA, tonB*) were grown overnight in LB broth, subculture into MOPS minimal media and grown to mid-log phase, exposed to the depolarizing agents CCCP or ColB for the indicated times, stained with DiOC2(3), and cytofluorimetrically analyzed for red fluorescence. Depolarization of the bacterial cytoplasmic

membrane results in an increase in red fluorescence of cell-associated DiOC2(3). CCCP depolarized both BN1071 and OKN13, whereas ColB only depolarized the former, *fepA+tonB+* strain, within 40 minutes of addition of the toxin. The figure shows the mean fluorescence values from two experiments, and the associated standard errors of the means. (Results collected by Dr. Phillip E. Klebba)

Temperature dependence of modification of genetically engineered Cys residues by FM

The experiments involved 25 existing Cys substitution mutations throughout FepA (37), and 10 new Cys substitutions in the N-domain (at residues 12, 39, 42, 51, 56, 59, 63, 101, 127, 135). In OKN3 (*fepA, tonB* +) the native *fepA* + promoter on pITS47 conferred wild-type expression levels for all the mutant proteins (Fig. 3.2; (37)). With the exception of W101C, the mutant proteins transported FeEnt like wild-type FepA in siderophore nutrition tests, and showed normal ColB susceptibility (data not shown). W101C sometimes formed an aberrant disulfide bond with the native Cys residues in L7 (Cys 487 and 494), which was seen in non-reducing SDS-PAGE (data not shown). We determined the accessibility of the sulfhydryl side-chains to FM labeling at 0°C and 37°C (Fig. 3.6 and Fig. 3.2). From studies of the concentration and time dependence of fluoresceination ((37); data not shown) we employed FM at 5 mM for 15 min in PBS, pH 6.5. This protocol primarily labeled the FepA mutant proteins, and other cellular proteins at lower levels, but not wild-type FepA (Fig. 3.2; Ma *et al*., 2007). To standardize the analysis of FM labeling we compared the fluoresceination of FepA to that of a cellular protein [band 3 in Fig. 3.2 (see also band 3 in fig. 3.3 of Ma *et al*., 2007)] that was

consistently modified throughout the experiments (mean among 20 independent samples, 7.7% _ 0.4% of total fluorescence in cell lysate proteins); we report the data as the ratio of fluorescence intensities: FepA-FL/ Band 3-FL (Fig. 3.6). When exposed to FM in the absence of ligands the reactivity of many FepA Cys side-chains was temperature dependent. At 0°C FM strongly modified Cys residues in the surface loops (101, 216, 271, 322, 383 and 698), and less intensely reacted with several sulfhydryl's in the N-domain (54, 56, 59, 63, 76) or at the periplasmic interface (residues 12, 14, 33, 666). Other residues in the N-domain (39, 92, 135), or on the interior (411, 565, 569, 585, 600) or exterior (367, 609) of the C-domain b-barrel were unreactive or only marginally labeled above background. Fluoresceination at many sites was temperature independent (residues 33, 54, 59, 216, 666), but modification of cell-surface Cys residues intensified as the temperature rose from 0°C to 37°C: nominally two- to threefold (residues 101, 216, 271, 383, 698), and as much as 7- to 10-fold (residues 63, 322, 470, 482, 550). These data suggested structural alterations in the loops in response to physiological temperature. Control reactions with bovine serum albumin (BSA) confirmed this inference: as temperature changed from 0°C to 37°C the maleimide modification of Cys in BSA only increased 26% (Fig. 3.6, inset), which corresponded to a Q10

temperature coefficient of 1.09 (Table 3.1). Thus the 200–1000% increase in loop residue labeling (Q10 values of 1.15–2.23) did not solely accrue from diffusion-controlled enhancement of the maleimide reaction rate, but rather, from conformational changes. It was noteworthy that enhanced chemical modification occurred in nine of the 10 surface loops that we tested (S63 in NL1; W101, NL2; T216, L2; S271, L3; A322, L4; A383, L5; S470, S482, L7; T550, L8, and A698, L11; S600 in L9 was not modified), which implied concerted conformational motion in the loops of FepA as temperature increased to physiological levels.

Effect of ColB binding and uptake on the accessibility of Cys residues to FM-labeling

At 0°C ColB only binds to FepA, whereas at 37°C it binds and kills the bacteria. We determined the susceptibility of sites within FepA to FM labeling in the presence of ColB (15-fold molar excess over [FepA]) at both temperatures. At 0°C toxin binding reduced modification (20–90%) at the following residues: 54, 56, 63, 101, 216, 271, 322, 383, 482 (Fig. 3.6 and Fig. 3.2). With the exception of G54 and N56, these sites exist within surface loops, and reduction of their modification at 0°C presumably originated from steric hindrance when ColB adsorbed to FepA. G54 and

N56 reside deeper within the N-domain, but may be labeled from the cell exterior (37), so ColB likely also obscured them by its surface binding. When we shifted cells with bound ColB to 37°C we observed few changes in the FM-labeling patterns (Fig. 3.6 and Fig. 3.2). As noted above, increasing the temperature augmented FM labeling of surface loop residues, but, just as at 0°C, incubation with ColB at 37°C generally impaired or blocked fluoresceination of these sites. For instance, modification of S63C in NL1 and T550C in L8, which was 10-fold more intense at 37°C, was virtually eliminated by the presence of the bacteriocin. ColB blocked all the same residues at 37°C that it blocked at 0°C. We looked for sites whose reactivity increased in response to incubation with ColB at 37°C, which was previously reported to occur from passage of the toxin through the FepA channel (2) but we did not observe any increase in FM modification for the 35 sites that we surveyed, including 15 in the N-domain. We saw no changes in residues 33, 42, 51 and 92, which Devanathan and Postle (2007) reported to increase in accessibility as a result of ColB penetration. At 13 of the 35 positions ColB had no effect on labeling; at the remaining 22 sites it decreased reactivity with FM. These latter residues were predominantly located in surface loops, but five positions in the globular domain also showed decreased

reactivity. None of these changes in Cys accessibility were TonB-dependent (see Effects of tonB), and likely resulted from steric hindrance during the interaction of the toxin with FepA. Because we did not observe ColB-induced increases in FM labeling during 30 min incubations, as reported by Devanathan and Postle (2007), and because we saw membrane depolarization within 5 min of exposure to ColB, we also performed experiments in which FM labeling initiated 1 min after exposure to ColB at 37°C, and continued for a 15 min duration. This protocol produced the same results: ColB blocked fluoresceination of the same residues, and did not increase the reactivity of any of the sites we surveyed (Fig. 3.6 and Fig. 3.2).

Effects of tonB on fluorescein labeling

ColB-mediated killing of *E. coli* requires TonB, presumably for passage of the toxin through the OM, so we expected to see TonB-dependent structural changes associated with colicin uptake [e.g. extrusion of the N-domain from the FepA channel (2) or other mechanistic dynamics]. We measured the reactivity of Cys residues in FepA in a *tonB* host strain in the absence and presence of ColB, and compared them with

the reactivity of the same residues in a *tonB* + host strain (Figs 3.6 and 3.3 and Figs 3.4 and 3.2).

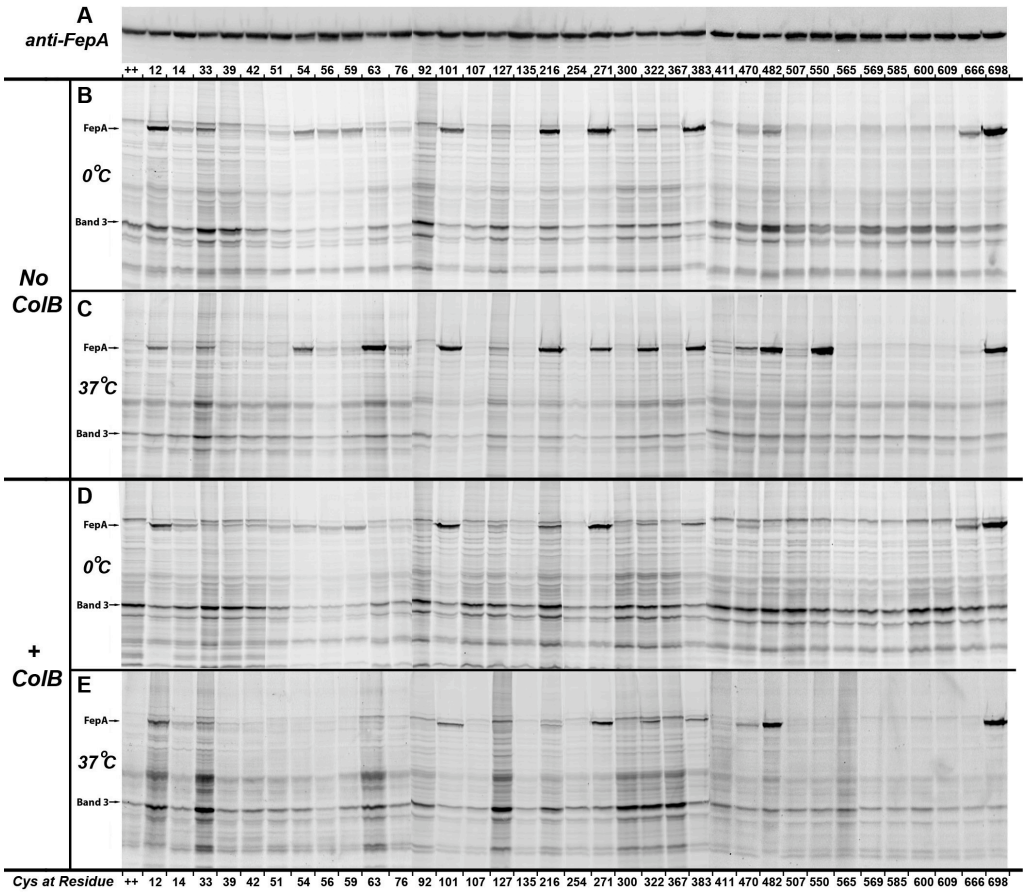

Figure 3.2 Representative images from scanned immunoblots and gels, which when quantified, produced Fig. 1. A. Expression.

Synthesis of FepA was visualized by anti-FepA immunoblots. SDS-PAGE gels of fluoresceinated cell lysates were transferred to nitrocellulose, incubated with anti-FepA MAb 45 (62), [125I]-protein A (36), and scanned on a StormScan phosphorimager. In this panel and B-E, the composite image joins 3 separate immunoblots or SDS-PAGE gels (gel 1:residues

12-76; gel 2: 92-383; gel 3: 411-698) that were scanned on a StormScanner (Molecular Dynamics).

B. FM-labeling at 0ºC. After harvest bacteria were chilled to 0ºC on ice, collected by centrifugation, resuspended in ice-cold PBS, incubated on ice for 30 min, and exposed to FM at 0ºC for 15 min.

C. FM-labeling at 37ºC. Cells were manipulated as in panel B, but after resuspension in cold PBS they were incubated for 30 min at 37ºC prior to exposure to FM at 37ºC for 15 min.

D. FM-labeling at 0ºC plus ColB. Cells were manipulated as in panel B, but exposed to a 15-fold excess of ColB (relative to [FepA]) for 30 min at 0ºC prior to exposure to FM at 0ºC for 15 min.

E. FM-labeling at 37ºC plus ColB. Cells were manipulated as in panel B, but exposed to a 15-fold excess of ColB (relative to [FepA]) for 30 min at 37ºC prior to exposure to FM at 37ºC for 15 min. In different conditions, cells expressing single Cys mutants showed differential FM labeling relative to the modification of Band 3 (37), which showed little variation in the samples (7.7 % ± 0.4% of total cellular fluorescence).

In the absence of ColB the main effect of the *tonB* locus was decreased fluoresceination of Cys residues in FepA (Fig. 3.3). However,

further analysis (see below) showed that the diminution resulted from lower FepA expression in the *tonB* host. Interaction with ColB at 37°C identically decreased the accessibility of Cys residues in the N-domain whether the target bacteria were killed by the toxin (*tonB*+) or immune to it (Δ*tonB*). In both strains we only saw reductions in fluoresceination associated with ColB binding, of the same magnitude and at the same sites. The absence of ColB-driven increases in the reactivity of 16 Cys substitutions in the globular domain, and the TonB independence of the ColB-associated decreases in fluoresceination suggested that Ton dependent structural changes do not occur during FepA–mediated ColB killing. James *et al*. (2008) reported that in the absence of ligands, binding of TonB to FhuA *in vitro* caused conformational changes in the surface loops of the receptor (1). Our fluoresceination procedures were appropriate to observe similar TonB-driven structural changes in FepA *in vivo*. We compared the reactivity of the panel of Cys residues in *tonB* +/– strains at 37°C, but we did not find differences in their reactivity in either the N-domain or the C-domain loops of FepA (Fig. 3.8). Again, FepA was expressed at lower levels in the *tonB* host: [125I]-protein A anti-FepA immunoblots revealed a 58% reduction in mean FepA expression level in OKN13 (*tonB*), relative to its expression level in OKN3 (*tonB* +).

Consequently, the engineered Cys sulfhydryl were less strongly labeled in the former strain. When we accounted for these protein concentration differences by determining the quantity of FepA (μg) in each sample (by [125I]-protein A anti-FepA immunoblots), the fluorescence intensities of the FepA bands per mg of FepA protein was the same in *tonB*+ or *tonB* host strains (Fig. 3.8). Hence, the relative fluorescence labeling levels of sites in both the globular domain and in the surface loops were the same whether TonB was present or absent.

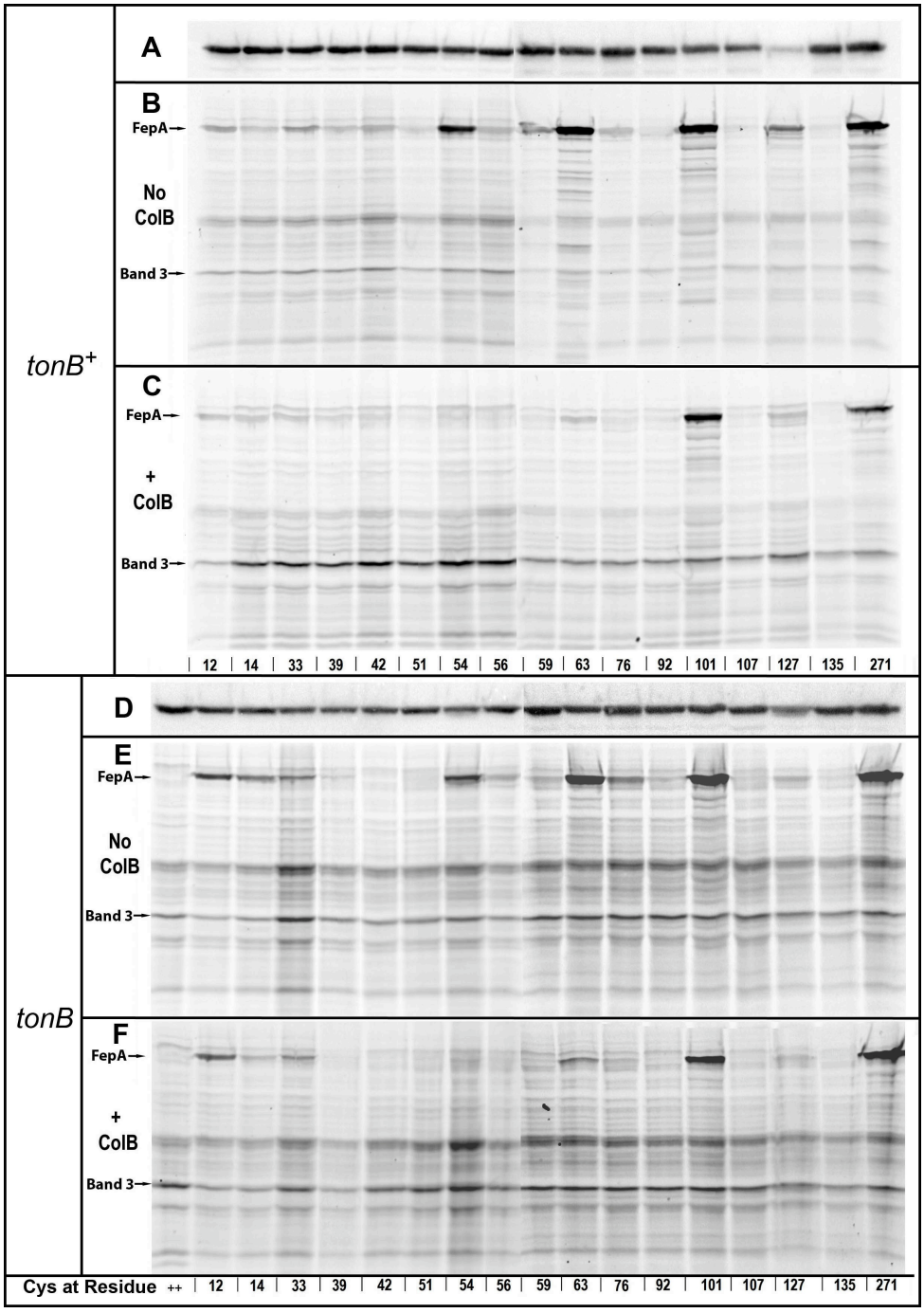
tonB+
A
B
FepA
No
ColB
Band 3
C
FepA
+
ColB
Band 3
12 14 33 39 42 51 54 56 59 63 76 92 101 107 127 135 271
tonB
D
E
FepA
No
ColB
Band 3
F
FepA
+
ColB
Band 3
Cys at Residue ++ 12 14 33 39 42 51 54 56 59 63 76 92 101 107 127 135 271

Figure 3.3 Representative images from immunoblots and gels, which when quantified, produced A and D.

Expression of FepA Cys mutants in OKN3 (*tonB+*; A*)* and OKN13 (*tonB*; D). Synthesis of FepA in was visualized as in Fig. S2. The images in these panels, and those in others in this figure, are composites from 2 separate immunoblots or gels (gel 1: residues 12-56; gel 2: 59-271); residue 271 is included as an internal positive control. The expression levels of wild-type FepA (++) and the Cys substitution mutant proteins (enumerated) were equivalent, but lower in OKN13 than in OKN3. **B. and C. FM-labeling of Cys mutant proteins in OKN3 at 37ºC, ± ColB.** Bacteria were prepared as in Fig. S2, but incubated at 37oC for 1 min in the absence (B) or presence (C) of ColB before FM was added for 15 min. E and F. FM-labeling of Cys mutant proteins in OKN13 at 37ºC, ± ColB. Cells were manipulated as Fig. S2: after resuspension in cold PBS they were incubated for 30 min at 37ºC in the absence (E) or presence (F) of ColB, prior to exposure to FM at 37ºC for 15 min.

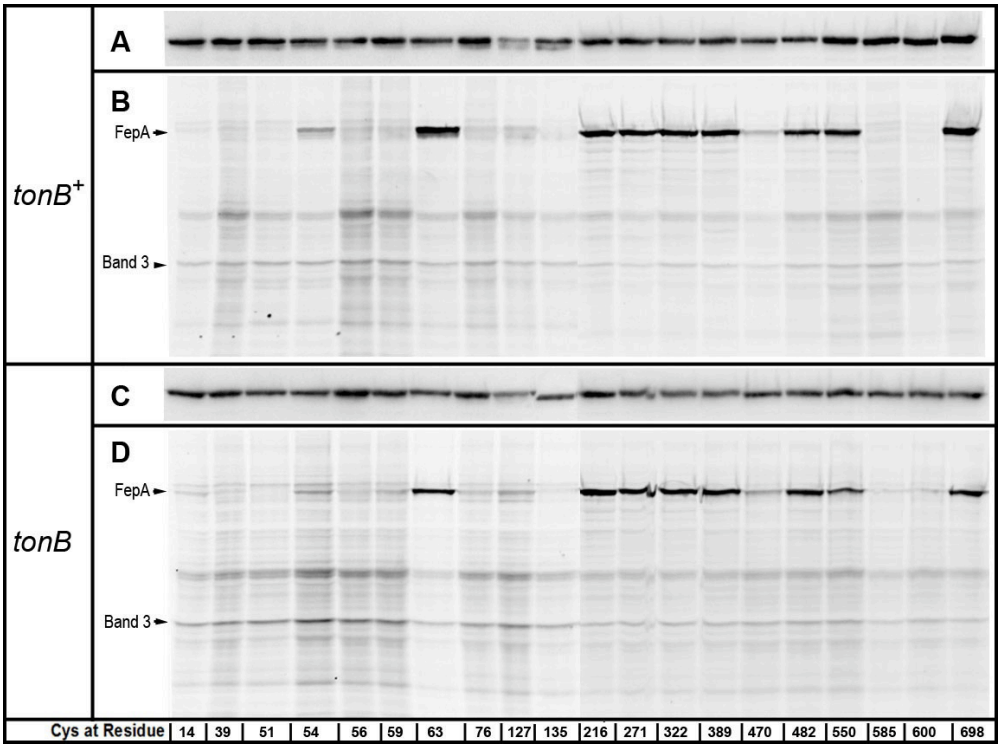

Figure 3.4 Representative images from scanned immunoblots and gels, which when quantified, produced Fig. 3. A and C. Expression of FepA Cys mutants in OKN3 (*tonB+*; A*)* and OKN13 (*tonB*; D).

Synthesis of FepA in was visualized as in Fig. S2. The images in these panels, and those in other panels in this figure, are composites from 2 separate immunoblots or gels (gel 1: residues 14-135; gel 2: 216-298). The expression levels of the Cys substitution mutant proteins (enumerated) were equivalent, but lower in OKN13 than in OKN3. **B and D. Comparison of fluoresceination of Cys side chains in OKN3**

(*tonB+*; B) and OKN13 (*tonB*; D) bacteria at 37ºC. Cells were manipulated as Fig. S2: after resuspension in cold PBS they were subjected to FM-labeling at 37ºC for 30 min.

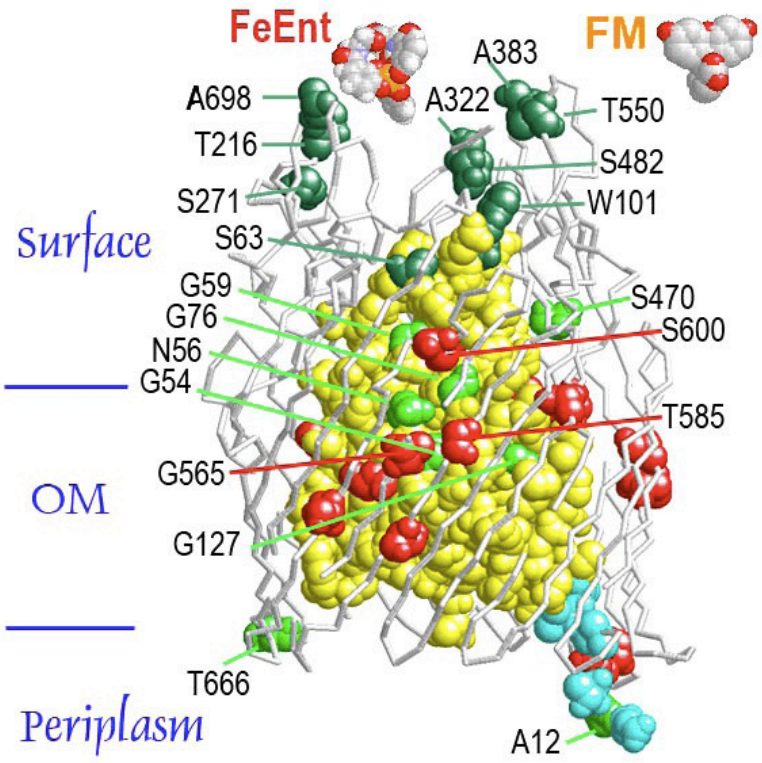

Figure 3.5 Relative accessibility of residues in FepA to modification by FM.

The N–domain is yellow and the C-domain is white; the TonB-box (amino acids 11- 17) is cyan. **Left.** The positions of 27 Cys substitutions (among a total of 35, 8 are not discernible in this view) are shown in space-filling format on a backbone representation of FepA tertiary structure. The most reactive residues are colored dark green, and less intensely

fluoresceinated residues are light green; for clarity, unreactive Cys substitutions (red) are not labeled.

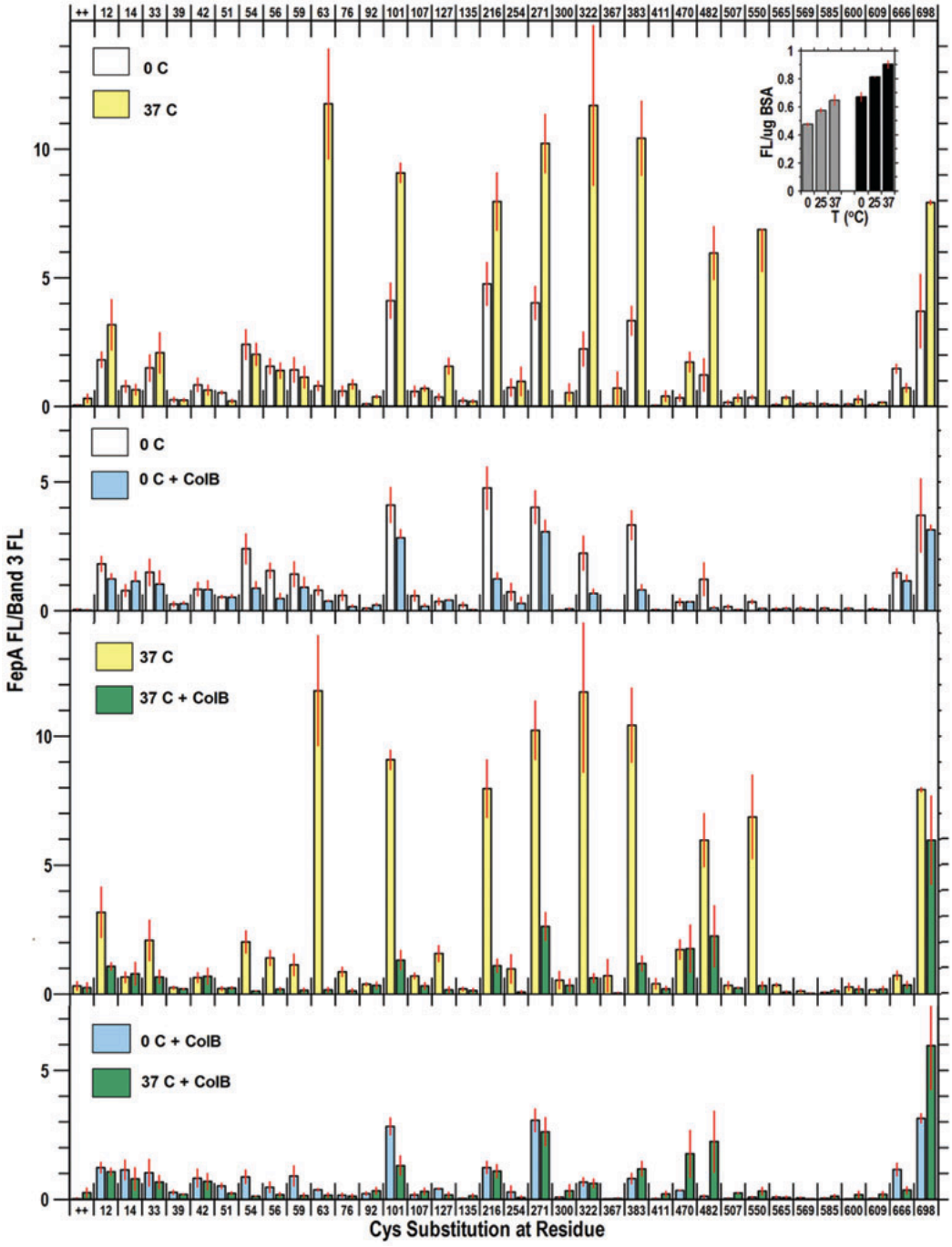
++ 12 14 33 39 42 51 54 56 59 63 76 92 101 107 127 135 216 254 271 300 322 367 383 411 470 482 507 550 565 569 585 600 609 666 698
0 C
37 C
0 C
0 C + ColB
37 C
37 C + ColB
0 C + ColB
37 C + ColB
FepA FL/Band 3 FL
Cys Substitution at Residue
FL/ug BSA
T (°C)
0 25 37 0 25 37

Figure 3.6 Accessibility of Cys residues in FepA to FM labeling at 0°C and 37°C, and during ColB binding (at 0°C) and uptake (at 37°C). OKN3 (*fepA*) harboring plasmids carrying *fepA* + or its derivatives that encode Cys substitutions mutations were prepared as described in *Experimental procedures*, resuspended in PBS, pH 6.5, and incubated for 30 min at 0°C or 37°C in the absence or presence of ColB, and then exposed to FM (5 mM) for 15 min at the same temperature. Cell lysates were resolved by SDS-PAGE and fluorescence images from the gels (Fig. S2) were analyzed by IMAGEQUANT (Molecular Dynamics). Each panel shows the mean FM labeling of FepA (relative to band 3) from three or more independent experiments, with associated standard error.

A. 0°C versus 37°C. White bars derive from cells labeled at 0°C; yellow bars are from cells labeled at 37°C. The inset shows fluoresceination of BSA at 0°C, 25°C and 37°C, in the presence of 5 mM (grey bars) and 50 mM (black) FM.

B. 0°C ± ColB. At 0°C the cells are metabolically inactive, so ColB binds but is not transported. White bars derive from cells labeled at 0°C in the absence of ColB; light blue bars are from cells labeled at 0°C in the presence of ColB.

C. 37°C ± ColB. At 37°C the cells are metabolically active, so ColB binds and kills. Yellow bars derive from cells labeled at 37°C in the absence of ColB; green bars are from cells labeled at 37°C in the presence of ColB.

D. 0°C versus 37°C, + ColB. The graph compares the effects of ColB on the labeling of FepA Cys mutants at 0°C and 37°C. No increases in FM labeling of N-domain residues were observed during ColB killing at 37°C.

Temperature dependence of modification of genetically engineered Cys residues by FM

The experiments involved 25 existing Cys substitution mutations throughout FepA (37), and 10 new Cys substitutions in the N-domain (at residues 12, 39, 42, 51, 56, 59, 63, 101, 127, 135). In OKN3 (fepA, tonB+) the native fepA+ promoter on pITS47 conferred wild-type expression levels for all the mutant proteins (Fig. 3.2; (37)). With the exception of W101C, the mutant proteins transported FeEnt like wild-type FepA in siderophore nutrition tests, and showed normal ColB susceptibility (need data here). W101C sometimes formed an aberrant disulfide bond with the native Cys residues in L7 (Cys 487 and 494), which was seen in non-reducing SDS-PAGE (performed by Vy Trinh).

We determined the accessibility of the sulfhydryl side-chains to FM labeling at 0ºC and 37ºC (Fig 3.6 and Fig. 3.2). Based on studies of the concentration and time dependence of fluoresceination (Ma et al., 2007; data not shown), we employed FM at 5 uM for 15 min in PBS, pH 6.5. This protocol primarily labeled the FepA mutant proteins, and other cellular proteins at lower levels, but not wild-type FepA (Fig. 3.2; (37)) To standardize the analysis of FepA to that of a cellular protein [band 3 in Fig. 3.2 (see also band 3 in fig. 3.8 of (37))] that was consistently modified

throughout the experiments (mean among 20 independent samples, 7.7% ± 0.4% of total fluorescence in cell lysate proteins); we report the data as the ratio of fluorescence intensities: FepA-FL/Band3-FL (Fig. 3.6).

When exposed to FM in the absence of ligands the reactivity of many FepA Cys side-chains was temperature dependent. At 0ºC FM strongly modified Cys residues in the surface loops (101, 216, 271, 322, 383 and 698), and less intensely reacted with several sulfhydryl in the N-domain (54, 56, 59, 63, 76) or at the periplasmic interface (residues 12, 14, 33, 666). Other residues in the N-domain (39, 92, 135), or on the interior (411, 565, 569, 585, 600) or exterior (367, 609) of the C-domain B-barrel were unreactive or only marginally labeled above background. Fluoresceination at many sites was temperature independent (residues 33, 54, 59, 216, 666), but modification of cell-surface Cys residues intensified as the temperature rose from 0ºC to 37ºC: nominally two- to threefold (residues 101, 216, 271, 383, 698), and as much as 7- to 10-fold (residues 63, 322, 470, 482, 550). These data suggested structural alterations in the loops in response to physiological temperature. Control reactions performed by Dr. Qiaobin Xiao with bovine serum albumin (BSA) confirmed this inference: as temperature changed from 0ºC to 37ºC the maleimide modification of Cys in BSA only increased 26% (Fig. 3.6, inset),

which corresponded to a Q_{10} temperature coefficient of 1.09 (Table 3.1). Thus the 200–1000% increase in loop residue labeling (Q_{10} values of 1.15–2.23) did not solely accrue from diffusion controlled enhancement of the maleimide reaction rate, but rather, from conformational changes. It was noteworthy that enhanced chemical modification occurred in nine of the 10 surface loops that we tested (S63 in NL1; W101, NL2; T216, L2; S271, L3; A322, L4; A383, L5; S470, S482, L7; T550, L8 and A698, L11; S600 in L9 was not modified), which implied concerted conformational motion in the loops of FepA as temperature increased to physiological levels.

Table 3.1 Temperature dependence of FM modification of engineered Cys sulfhydryl in the surface loops of FepA

Residue	Loop	Q_{10}
BSA		1.09
63	NL1	2.07
101	NL2	1.24
216	L2	1.15
271	L3	1.29
322	L4	1.56
383	L5	1.36
470	L7	1.55
482	L7	1.53
550	L8	2.23
698	L11	1.23

Data from the top panel of Fig. 1 were used to calculate the Q_{10} temperature coefficient (93), according to the relationship

$$Q_{10} = \left(\frac{R_2}{R_1}\right)^{10/(T_2 - T_1)}$$

where R is the rate (extent of fluoresceination) and T is the temperature in ºC. For BSA, Q_{10} was invariant whether FM was employed at 5 μM (1.087) or 50 μM (1.084) [Data by Qiaobin Xiao].

Effect of ColB binding and uptake on the accessibility of Cys residues to FM labeling

At 0°C ColB only binds to FepA, whereas at 37°C it binds and kills the bacteria. We determined the susceptibility of sites within FepA to FM labeling in the presence of ColB (15-fold molar excess over [FepA]) at both temperatures. At 0°C toxin binding reduced modification (20–90%) at the following residues: 54, 56, 63, 101, 216, 271, 322, 383, 482 (Fig. 3.6 and Fig. 3.2). With the exception of G54 and N56, these sites exist within surface loops, and reduction of their modification at 0°C presumably originated from steric hindrance when ColB adsorbed to FepA. G54 and N56 reside deeper within the N-domain, but may be labeled from the cell exterior (37), so ColB likely also obscured them by its surface binding. When we shifted cells with bound ColB to 37°C we observed few changes in the FM-labeling patterns (Fig. 3.6 and Fig. 3.2). As noted above, increasing the temperature augmented FM labeling of surface loop residues, but, just as at 0°C, incubation with ColB at 37°C generally impaired or blocked fluoresceination of these sites. For instance, modification of S63C in NL1 and T550C in L8, which was 10-fold more intense at 37°C, was virtually eliminated by the presence of the bacteriocin. ColB blocked all the same residues at 37°C that it blocked at

0°C. We looked for sites whose reactivity increased in response to incubation with ColB at 37°C, which was previously reported to occur from passage of the toxin through the FepA channel (2) but we did not observe any increase in FM modification for the 35 sites that we surveyed, including 15 in the N-domain. We saw no changes in residues 33, 42, 51 and 92, which Devanathan and Postle (2007) reported to increase in accessibility as a result of ColB penetration. At 13 of the 35 positions ColB had no effect on labeling; at the remaining 22 sites it decreased reactivity with FM. These latter residues were predominantly located in surface loops, but five positions in the globular domain also showed decreased reactivity. None of these changes in Cys accessibility were TonB dependent (see below), and likely resulted from steric hindrance during the interaction of the toxin with FepA.

Because we did not observe ColB–induced increases in FM labeling during 30 min incubations, as reported by Devanathan and Postle (2007), and because we saw membrane depolarization within 5 min of exposure to ColB, we also performed experiments in which FM labeling initiated 1 min after exposure to ColB at 37°C, and continued for a 15 min duration. This protocol produced the same results: ColB blocked

fluoresceination of the same residues, and did not increase the reactivity of any of the sites we surveyed (Fig. 3.7 and Fig. 3.3).

Effects of TonB on FM labeling

ColB-mediated killing of *E. coli* requires TonB, presumably for passage of the toxin through the OM, so we expected to see TonB-dependent structural changes associated with colicin uptake [e.g. extrusion of the N-domain from the FepA channel (2) or other mechanistic dynamics]. We measured the reactivity of Cys residues in FepA in a *tonB* host strain in the absence and presence of ColB, and compared them with the reactivity of the same residues in a *tonB* + host strain (Figs 1 and 2 and Figs 3.3 and 3.2).

In the absence of ColB the main effect of the *tonB* locus was decreased fluoresceination of Cys residues in FepA (Fig. 3.3). However, further analysis (see below) showed that the diminution resulted from lower FepA expression in the *tonB* host. Interaction with ColB at 37°C identically decreased the accessibility of Cys residues in the N-domain whether the target bacteria were killed by the toxin (*tonB*+) or immune to it (Δ*tonB*). In both strains we only saw reductions in fluoresceination associated with ColB binding, of the same magnitude and at the same

sites. The absence of ColB-driven increases in the reactivity of 16 Cys substitutions in the globular domain, and the TonB independence of the ColB-associated decreases in fluoresceination suggested that TonB-dependent structural changes do not occur during FepA-mediated ColB killing.

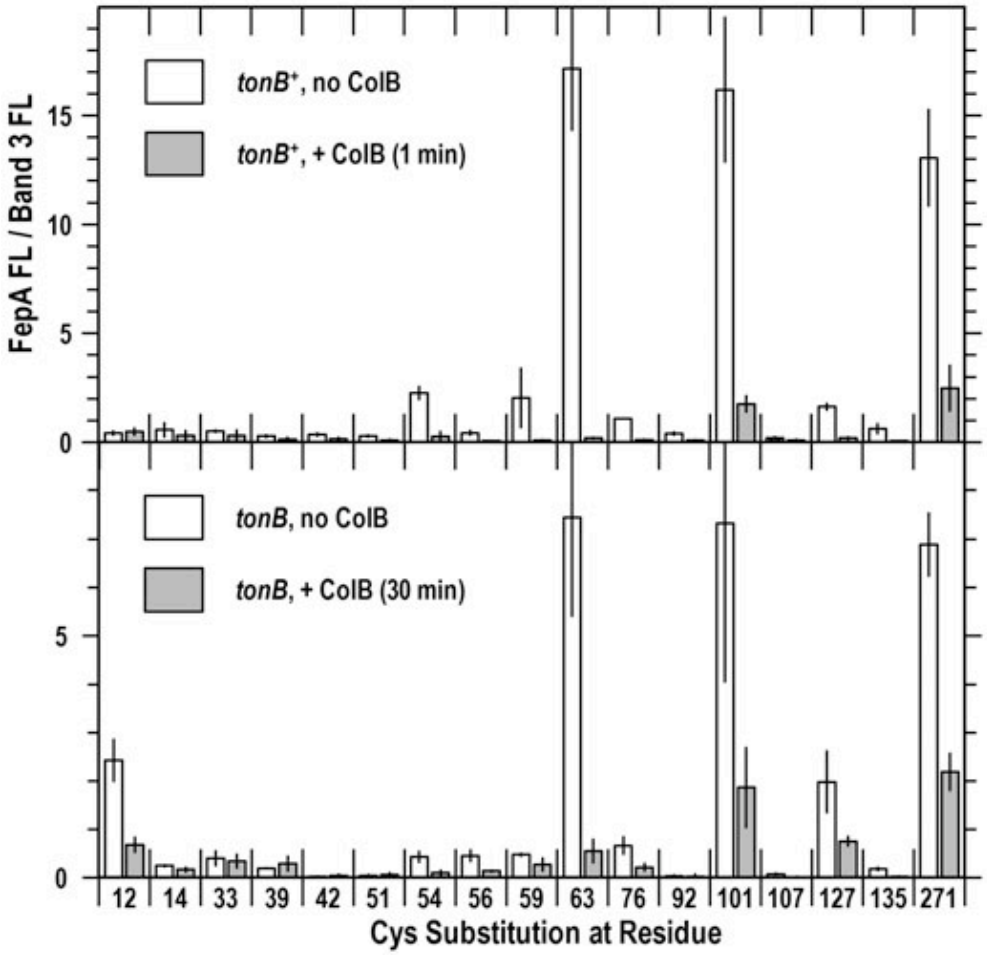

Figure 3.7 Effects of ColB exposure time and TonB on the fluoresceination of N-domain Cys residues in FepA.

SDS-PAGE gels of cell lysates (Fig. S3) were scanned on the fluorescence imager and analyzed by IMAGEQUANT (Molecular Dynamics). Bars show the mean FM labeling of FepA (relative to band 3) from two or three independent experiments, with associated standard error. Top. 1 min exposure of *tonB* + cells to ColB. OKN3 harboring

plasmids carrying *fepA* + or its Cys substitution derivatives were subjected to FM labeling as in Fig. 1, except that cells were incubated for only 1 min at 37°C in the absence (white) or presence (grey) of ColB, prior to labeling with FM (5 mM; 15 min; 37°C). Bottom. 30 min exposure of *tonB* cells to ColB. OKN13 (*tonB, fepA*) carrying *fepA* + or its Cys substitution derivatives was incubated for 30 min at 37°C in the absence (white) or presence (grey) of ColB, prior to exposure to FM at 37°C for 15 min.

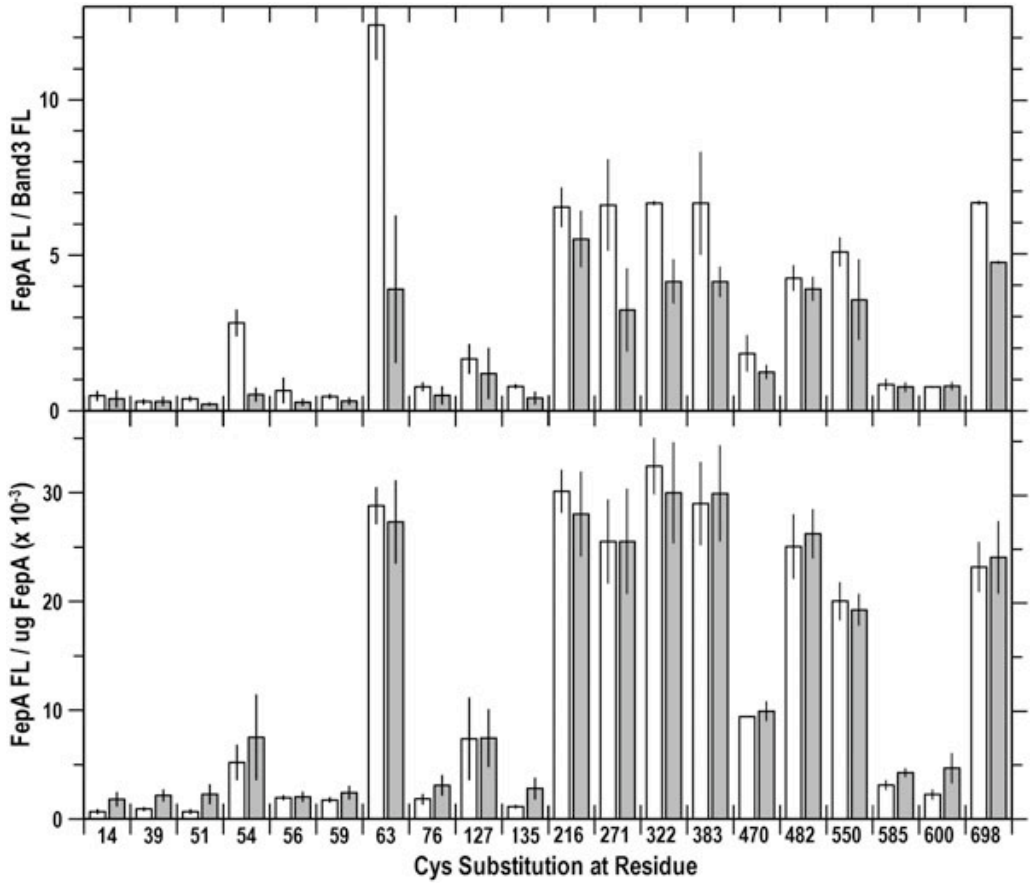

Figure 3.8 Evaluation of TonB-dependent conformational changes in FepA: Comparison of Cys fluoresceination in *tonB* + and *tonB* cells.

Sites in FepA that were significantly labeled by FM were re-analyzed and compared in *tonB* + (white bars) and *tonB* (grey bars) cells. We incorporated the concentration of FepA (from anti-FepA immunoblots) into calculations to compare the relative and absolute FM labeling levels. **Top.** Relative levels of FM labeling in *tonB* + and *tonB* bacteria. Fluorescence

images from SDS-PAGE gels of cell lysates were analyzed by IMAGEQUANT (Molecular Dynamics). Bars depict the mean FM labeling of FepA proteins relative to band 3 in OKN3 (white) and OKN13 (grey; mean of three experiments, with associated standard error). FepA proteins were less fluoresceinated in the *tonB* strain, because they were expressed at lower levels (Fig. S4). **Bottom.** Absolute levels of FM labeling in *tonB*+ and *tonB* strains. The extent of residue labeling was corrected for the expression level of each of the mutant FepA protein, to yield the absolute labeling level (fluorescence intensity/mg FepA). The correction eliminated the differences in labeling between *tonB*+ and *tonB* cells seen in the top panel.

Discussion

The differential labeling of engineered Cys sulfhydryl groups by FM reflects their chemical accessibility. The changing chemical modification patterns document structural states in FepA: at different temperatures, during its interaction with ColB, and in the presence or absence of TonB. Enhanced fluoresceination at 37°C reflects greater reactivity of Cys sulfhydryl groups in certain locations, and this greater chemical accessibility inferred conformational changes in surface-exposed regions of the receptor as the conditions warmed to physiological levels. Loop motion was previously seen by site-directed spectroscopy (26,35,41,94), by the disordered nature of L4, L5 and L7 in FepA crystal structure (27), and by transitions in FepA (26,31) and FecA (42) from open forms that adsorb ligands to closed forms that subsequently transport them. Fluoresceination was highly temperature dependent at certain sites (S63C, T550C), which had Q10 values of approximately 2 (a doubling of reaction rate for each 10 degree increment in temperature). These data imply loop conformational motion as the temperature rises (93). Fluoresceination of BSA only slightly increased at 37°C, and Cys sulfhydryl at other sites in FepA (residues 14, 42, 54, 56, 59, 76, 107, 254, 666) were much less, or unaffected by the change to 37°C. Hence, the

increased chemical modification of the loops at 37°C reflects conformational dynamics that allow better permeation of the reagent. The simplest explanation is that higher temperatures open or relax the loops of FepA, increasing their permeability to small molecules. The hydrophobicity and negative charge of FM roughly mimic FeEnt: it's an aromatic, anionic probe with slightly smaller dimensions (427 Da versus 716 Da), so ingress of the fluorophore into FepA structure may reflect the natural movement of FeEnt during transport. These experiments do not define the range of motion, because virtually any alteration of protein architecture may enhance the accessibility of a small reagent to the target sites. But, they indicate, for the first time, that as the cell warms L2, L3, L4, L5, L7, L8 and L10 of FepA undergo concerted conformational change, potentially improving receptor activity by increasing ligand interactions with relevant amino acid side chains (29,49). FepA has 100-fold higher affinity for FeEnt *in vivo* (*K*d = 0.1 nM; (29,36,49)) than *in vitro* (*K*d = 10 nM; (26)), and the receptor's conversion between open and closed forms may contribute to these differences.

The mechanism of OM penetration by colicins (assuming that they enter by a common mechanism) is unknown: do they pass the OM by transit through porin channels, or by a more obscure transport process? In

their analysis of the interaction between ColB and FepA, Devanathan and Postle (2007) used different reagents and methodologies to conclude that the bacteriocin traverses the receptor's transmembrane channel. Our results do not support this interpretation: we found no evidence of ColB passage through the FepA pore. Whereas Devanathan and Postle (2007) considered the accessibility of 12-engineered Cys residues in the N-terminal globular domain of FepA; we studied 35 sites dispersed throughout its tertiary structure: 16 in the N-domain and 19 in the C-terminal b-barrel. Four substitutions were common to both studies (at A33, A42, T51 and S92). Devanathan and Postle (2007) reported increased modification of the N-terminal most six sites in the globular domain (T13, S29, A33 A42, S46, T51) when cells were exposed to excess ColB (fourfold) at 37°C for 30 min (2). Conversely, we saw no increases in the modification of any FepA residues, including the four common sites. The discrepancies in the results may originate from the different methodologies. Devanathan and Postle (2007) used a catenation of reagents and procedures: after exposure to 1-biotinamido-4-[4′-(maleimidomethyl) cyclohexanecarboxamido] butane (BMCC), they lysed the cells, solubilized membrane proteins with detergent, immunoprecipitated FepA with an anti-FepA antibody, subjected the

immunoprecipitates to SDS-PAGE, transferred the resolved proteins to nitrocellulose, stained them with avidin-horseradish peroxidase, and 'The extent of labeling *in vivo* for each FepA Cys substitution was estimate visually.' Measurement of chemical reactivity in the periplasm depends on passage of the reagent through the OM. Devanathan and Postle (2007) used BMCC: its mass of 534 Da is near the exclusion limit of *E. coli* general porins (95), and its extended molecular dimension (Stoke's diameter of 34 Å) is threefold greater than the diameter of the OmpF channel (96). These considerations make its OM transport problematical and much slower than that of FM, which is 20% smaller in mass (427 Da) and compact (Stoke's diameter of 10 Å). FM traverses the OM via porin channels and efficiently labels sulfhydryl in the periplasm (37). On the other hand, visualization of BMCC labeling in the periplasm required high concentrations of the reagent (93 mM, about 20-fold higher than that of FM in our experiments), combined with amplified immunochemical and enzymatic procedures. We cannot fully explain the conflicting results of the two studies, but the methodological differences are likely responsible. Our experiments exposed bacteria to FM, lysed them in SDS sample buffer, subjected the lysates to SDS-PAGE, and measured fluorescence intensity on a phosphorimager. These simpler procedures and fewer

manipulations created less opportunity for adventitious error, and produced better fluorescent images, whose analysis yielded statistical measures of reproducibility. We expected the methodologies to accurately detect differences in reactivity at specific sites, and the range of fluorescence labeling that we found in response to temperature and ColB binding confirmed this expectation.

Exposure to ColB at 37°C slightly decreased the labeling of side-chains in the interior or on the periplasmic surface of FepA (residues 12, 14, 54, 56, 59, 76 and 127), suggesting that during the ColB killing phase the structure of FepA remains closed and less accessible to the extrinsic fluorophore. Shorter incubation times with ColB and equivalent experiments in a *tonB* strain produced identical results: the same residues were labeled to the same relative extent at 37°C in the absence and presence of ColB. Thus, our results show no indication of ColB passage through the FepA channel. We also note, however, that once excess ColB saturates FepA on the cell surface, we know neither how many colicin molecules successfully traverse the OM and depolarize the IM, nor how long thereafter ColB transport continues, before energy depletion terminates the process. The single hit-killing mechanism of bacteriocins (97) raises the possibility that only one or a few ColB molecules per cell

breach the OM barrier, and in this case we do not anticipate gross changes in the FM-labeling pattern of FepA, which is present at a level of approximately 40,000 chromosomally encoded receptors per cell (36,49). Finally, we did not observe any TonB-dependent fluctuations in FM-labeling levels at the sites we analyzed in FepA. These results differ from the behavior of FepA during FeEnt transport, where Ton dependent labeling of residue G54C from the periplasmic space implied extrusion of the N-domain during the metal transport reaction (37).

Chapter 4 : Analysis of FepA conformational loop motion during binding and transport of FeEnt

Background

The binding of FeEnt to FepA has been shown to be a high affinity process (Kd ≈ 10^{-10} M), which involves the participation of multiple sites in the FepA loops and N-domain (29,49). Without the ligand, loops of FepA exhibit flexible motion (31) and the conformation of the surface loops are susceptible to temperature changes (40). During ligand binding the FepA surface loops likely undergo two states of binding, from the initial binding phase (B1) to a secondary state (B2) when the loops ensconce the ligand for uptake into the N-domain (26).

The high-affinity recognition of FeEnt, the catecholate-containing siderophore, involves numerous aromatic and basic residues of the FepA surface loops (49). FepA loop deletion studies severely inhibited the binding and uptake of FeEnt, which indicated that loops L7 and L8 are essential for the uptake of the ligand (36). The substitution of aromatic residues located in L7 (Y481, Y478, Y495) (49) and severe effects from the deletion of L7, suggests a special role for loop L7 and support roles for loops adjacent to L7.

Despite numerous methods to probe FepA binding and transport mechanism in live cells, including recent fluor accessibility studies (37,40) that provided insight on global structural aspects of FepA, the ligand binding and transport mechanism remains unresolved. Surface loops of FepA are proposed to undergo two successive conformational changes during a biphasic FeEnt binding (26) event to subsequently transport into the periplasm. For instance, FeEnt may initially bind to accessible loops that would induce subsequent binding events in each adjacent loop prior to uptake of the ligand through the N-domain. Using fluorescence spectroscopy in live cells, rates of fluorescence change time course curves were collected from individual loops. Single Cys mutation sites were designed and labeled with FM based on previous studies of FepA surface loops to determine loop conformational motion during the FeEnt uptake mechanism. These loop mutants were also characterized by radioisotopic binding and transport data to determine if the single Cys sites or the FM label affected the affinity of FepA (Figs. 4.3, 4.4). We observed unique fluorescence changes character within the FepA surface loops and classified the loop conformational changes into two groups, with L7 exhibiting a central role during the FeEnt uptake mechanism. Consequently, these results favored an entry point for the ligand into the

N-terminal globular domain centered on FepA loop L7. The fluorescence quenching character in the absence and presence of the IM protein TonB provided further validity to the two-state binding mechanistic model previously proposed by Payne et al.(26). Furthermore, rates of fluorescence change of individual loops occurred much faster when IM protein TonB was absent, these results suggest that the surface loop conformation is dependent on TonB action within the FepA N-domain.

Results

Host cells OKN3 (fepA–, tonB+) or OKN13 (fepA–, tonB–) harboring pits23 expressing FepA with Cys mutations were suspended in 2mLs of MOPS buffer containing 0.4% glucose with a concentration of $2.5x10^7$ cells/mL with constant mixing at 25ºC. We aligned the raw fluorescence time course readings (Fig. 4.1) from each individually FM-labeled sample with the insertion of 10nM FeEnt at 300 seconds (Fig 1.). The aligned time courses were averaged and normalized to percent fluorescence for each FepA Cys loop mutant T216C–L2, S271C–L3, A322C–L4, A383C–L5, S490C–L7, T550C–L8, and A698C–L11 (Fig 4.2). Normalized percent fluorescence displayed different extents of quenching and sequential recovery of fluorescence agreed with previous

spectroscopic observations (35). The normalized fluorescence time course results revealed that fluorescence recovery was dependent on the concentration of the ligand for each individual loop mutation (Fig. 4.3). With cell concentrations maintained at $2.5x10^7$ cells/mL and concentrations of FeEnt introduced at specific time points, significantly less extents of quenching were observed, and recovery times were also faster, for lower concentrations of the ligand due to substrate depletion. With the ligand concentration of 10nM, normalized fluorescence readings of each loop mutant revealed two distinct groups of fluorescence changes, Group A (L2, L3, L11) exhibited large extents of quenching with fast recovery rates and Group B (L4, L5, L7, L8) exhibited smaller extents of quenching, with an exception for L7. However, all Group B loop exhibited much slower rates of recovery than Group A. Furthermore, sequentially decreasing rates of recovery were observed from Group A side of the FepA surface loop domain to the Group B loop side (Table 4.2).

Double exponential fits of the fluorescence quenching provided two rate constants for loop conformational motion (k1 and k2). We interpreted k1 and k2 rate constants into a two-state binding mechanism of conformational motion and calculated rates B1 and B2 (Table 4.1). The initial binding state (B1) is the binding of the ligand that occurs in the

extremities of the loops, and the secondary binding state (B2) is a conformational state that involves residues at the base of the loops and in the N-domain that must occur before the uptake of ligand into the N-domain. Overall B1 rates were faster than B2 rates, with one exception in L11 where the rate of quenching was equal for the two binding states (Fig. 5b). The largest extent of quenching (i.e. range of conformational motion) was consistently observed in L11 of FepA (see Fig. 4.2); L11 being the loop with the longest reach when viewed in the crystal structure of FepA (Fig. 4.5). Although, the extents of quenching for Group A loops could be attributed to the size of each loop, upon closer inspection of the crystal structure, L7 and L8 are approximately the same length as L2 and L3, but display very distinctly different fluorescence changes. Therefore, Group A loops must be involved in multiple roles during ligand uptake. Interestingly, the two different groups of loop fluorescence changes are on completely opposites sides of the FepA vestibule when (Fig. 4.5). Fluorescence recovery for each individual loop were reciprocated by the negative logarithmic equation and fitted to single exponential decays (Table 4.1).

Effects of fluor attachment on loop conformational motion

The effects of covalent modification of Cys residues of FepA surface loops in living cells were measured by radioisotopic biochemical binding and transport assays using 59FeEnt (Table 4.4). Binding capacity is representative of the total amount of available sites for ligand binding compared to the wild type. The single sulfhydryl mutations introduced in the loops of FepA did not significantly inhibit the binding or transport of all sites tested. Mutations A322C–L4 and A383C–L5 displayed significant decreases in FeEnt transport function without the presence of the fluor label. These decreased levels of binding and transport functionality emphasize the importance of L4 and L5 in the FepA surface loops uptake of FeEnt. Decreased binding capacity for FM-labeled mutants implied that the presence of the fluor label in the surface loops of FepA prevents optimal binding at multiple sites, and increases in severity for loops more proximal to L7. However, there were some exceptions in the decreased binding capacity trends for L11 and L3, which show no decrease and an increase in binding capacity, respectively. The most dramatic effect in binding capacity was seen for the mutant A383C–L5, and implied that L5 appears to be required for optimal binding of the ligand. Surprisingly, only minor differences were observed for the Km of unlabeled loop mutants

compared to FM-labeled loop mutants (Table 4.4). The Km for FM-modified L4 and L5 loops displayed the most significant effects during binding, which were affected more than most, but still in the ideal nM range for ligand binding and therefore not significant detriment to the overall function of uptake. On the other hand, decreased Vmax values were significant for most loops modified with the fluor attachment. The Vmax transport data clearly indicated the fluor attachment does affect the functionality of FepA, fluorescence changes, and therefore the extent of conformation motion of the individual FepA surface loops. Recovery rates, indicative of FeEnt uptake efficiency in FepA, were compared with ^{59}FeEnt transport assay results to compare FepA transport functionality. FepA transport functionality comparison form the two different methods (Fig. 4.6) revealed the ability of fluorescence spectroscopy to report individual loops compared to a global perspective within FepA uptake due to the fluor attachment. Comparing the results from each method revealed differences for Group A loops duration of FeEnt uptake, whereas FeEnt uptake for the fluorescence recovery assay was typically much faster than radioisotopic counts of FeEnt uptake. Furthermore, Group B loops, specifically L7 and L8, exhibited equal duration times for transport. It is worth mentioning that we also designed two single cysteine mutations

(G640C, T648C) in L10, and observed no fluorescence responses and severe defects of binding and transport ability (data not shown).

Effects of fluorescence quenching in the tonB background

Effects of fluorescence quenching for two-state binding in the absence of TonB revealed faster rates of conformational motion, rates were equal except in loops L3, L4, and L5 (Fig. 4.1). L3 and L4 exhibited slower secondary rates of motion in tonB– background, the reverse character was observed in L5, which suggests conformation of the FepA loops are different when TonB is absent. The rates for L8 and L11 remained unchanged for the two binding events regardless of TonB presence. Quenching rates for loop mutants in tonB– background were overall faster with a few exceptions the only exception in L5 (Table 4.1). In collusion with ^{59}FeEnt binding and transport data, the rates of quenching imply that conformational loop motion is dependent on the presence of TonB. Equal extents of quenching between TonB+ and TonB– FM-labeled FepA mutants were observed for most mutants (Fig. 4.4). However, we measured a consistent 20% decrease in the extent of quenching between the two backgrounds for A698C–L11. This result indicated that the extent of motion for the largest loop was not as great in the tonB– background

and therefore the conformation of the FepA surface loops may be different when TonB is absent.

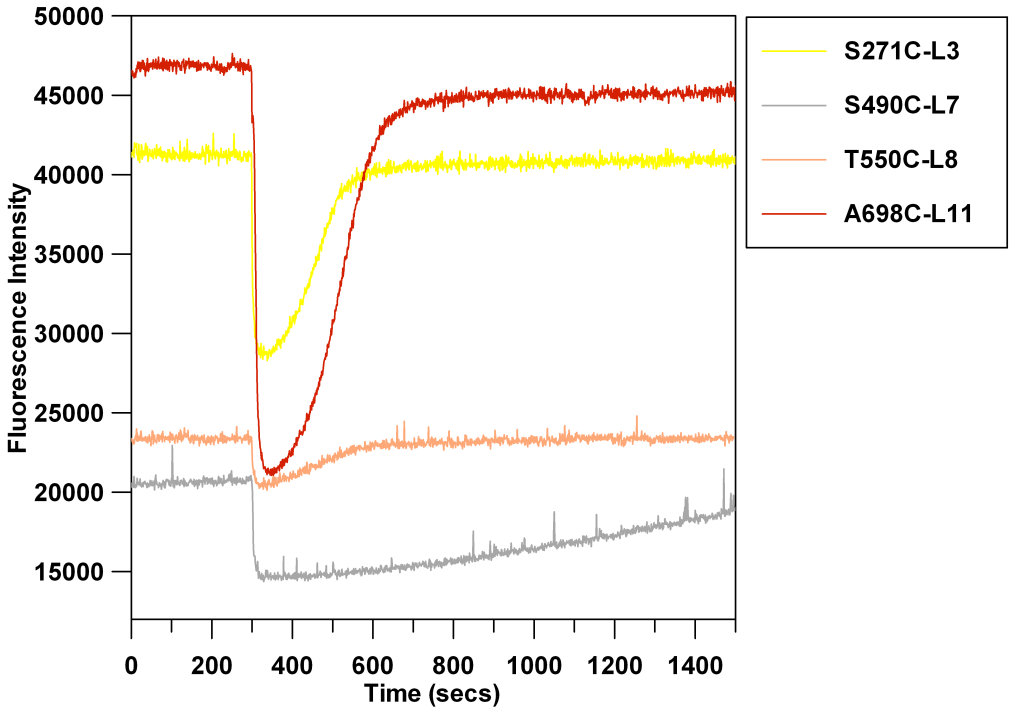

Figure 4.1 Raw fluorescence spectroscopy results.

We aligned the raw fluorescence time course from each individually FM-labeled sample with the insertion of 10nM FeEnt at 300 seconds. Cell concentration was kept constant at 2.5×10^7 cells/mL suspended in MOPS with 0.4% glucose. Time course fluorescence tracings are S271C–L3 (yellow), S490C–L7 (grey), T550C–L8 (flesh), and A698C–L11 (dark red). The data were analyzed and plotted in GraFit 6.0.1.

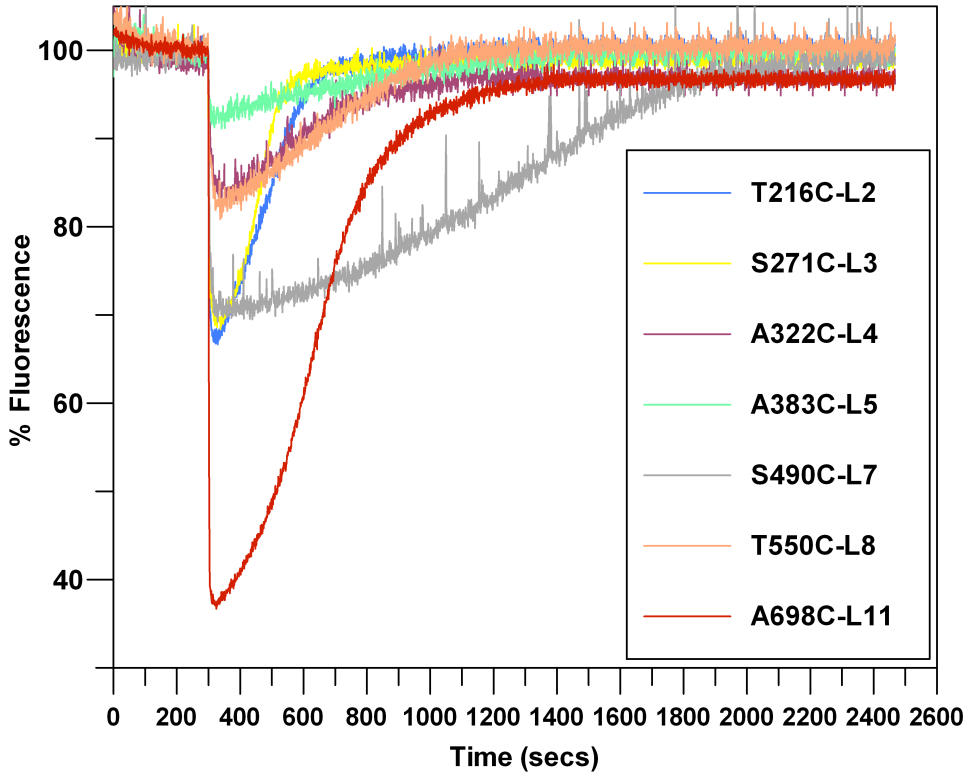

Figure 4.2 Normalized fluorescence time course of individual FM-labeled FepA surface loops.

OKN3 cells harboring pits23-expressing FepA with single Cys mutation were suspended in 2mL of MOPS buffer containing 0.4% glucose with cell concentration of 2.5×10^7 cells/mL with constant mixing at 25ºC. The raw fluorescence time course were aligned by ligand insertion, averaged, and normalized to percent fluorescence for each FepA Cys loop mutant T216C–L2 (blue), S271C–L3 (yellow), A322C–L4 (purple), A383C–L5 (sea green), S490C–L7 (grey), T550C–L8 (flesh), and A698C–L11 (dark

red). Normalized percent fluorescence displays different extents of quenching and sequential recovery of fluorescence. The data were analyzed and plotted in GraFit 6.0.1.

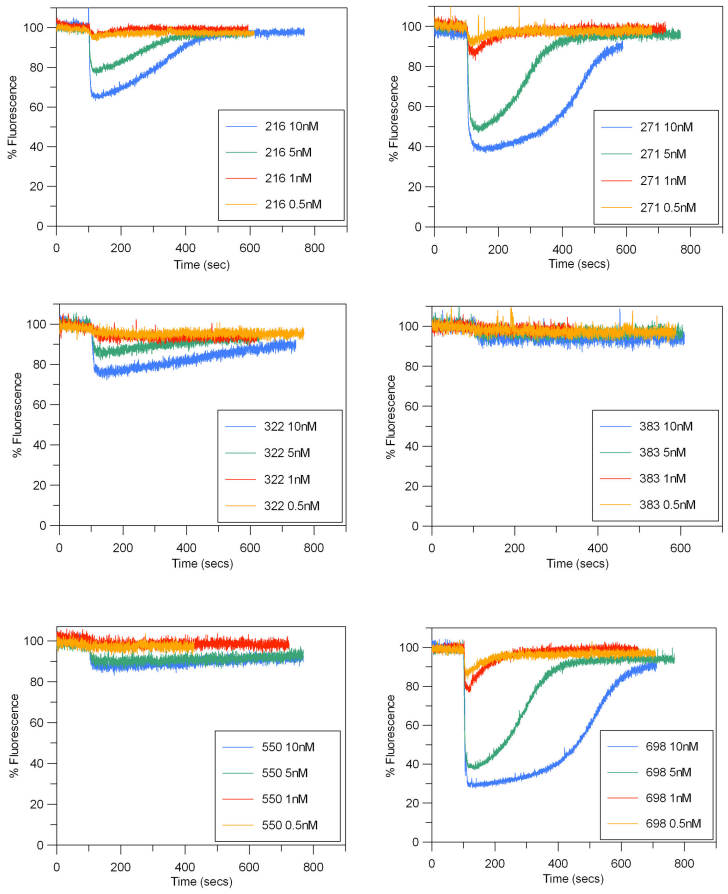

Figure 4.3 FeEnt Concentration dependence of Fluorescence Quenching.

Previous spectroscopic observations (35) were verified in each individual mutation. The fluorescence recovery is dependent on the concentration of the ligand for each individual loop mutation. Cell concentration was maintained at 2.5×10^7 cells/mL and concentration of FeEnt. Due to

substrate depletion at lower concentrations of the ligand, extent of quenching is much less and recovery time was fast. Data were analyzed and plotted in GraFit 6.0.1.

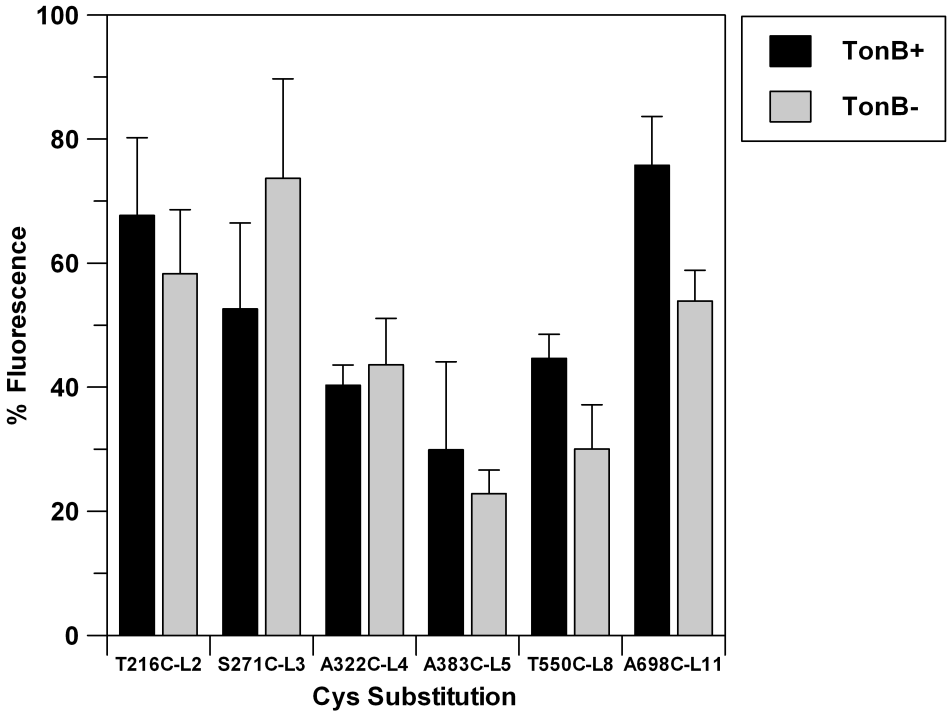

Figure 4.4 Extent of Fluorescence Quenching.

The average extent of quenching from the percent fluorescence plots displayed sequentially decreasing extents of quenching from Group A (L2, L3, L11) side of the FepA loop domain to the Group B (L4, L5, L8) side. Equal extents of quenching were observed for most FM-labeled FepA mutants in the TonB+ (black bars) background compared to the TonB–

(grey bars) background. The 20% decrease in the extent of quenching between the two backgrounds in A698C–L11 was due to the absence of TonB. Also, Group B (L2, L3, L11) sites quench to the same extent in the absence of TonB.

Table 4.1 Fluorescence rates of FeEnt uptake for multiple FM-labeled sites in FepA loops

	Quenching[a]				Recovery[b]
	tonB+		tonB–		Half-life
Mutant–Loop	B1 (secs)	B2 (secs)	B1 (secs)	B2 (secs)	$t_{1/2}$ (secs)
T216C–L2	1.34	6.21	1.30	1.29	103
S271C–L3	5.85	8.10	4.44	6.67	68
A322C–L4	1.15	4.67	3.79	11.85	192
A383C–L5	1.83	3.46	3.94	1.69	630
S490C–L7	2.10	2.16	1.41	1.43	1123
T550C–L8	2.77	3.26	2.55	2.78	315
A698C–L11	6.09	5.69	2.60	2.62	165

a. Rate of fluorescence quenching by insertion of FeEnt (50nM) provided two rates of loop conformational motion in OKN3 (tonB+ background) and OKN13 (tonB– background) for multiple labeled sites. B1 and B2 rates are half-life rates (seconds) calculated in GRAFIT 6.0 (Erithacus Software) from 'double exponential' rate constants k1 and k2 of the fluorescence quenching time course curves during FeEnt (50nM) uptake.

b. Fluorescence recovery half-life rates (seconds) were obtained from fluorescence time course curves that were reciprocated and fitted to 'single exponential decay' equation in GRAFIT 6.0 (Erithacus Software). Recovery rates are indicative of transport efficiency and should agree with ^{59}FeEnt uptake results

Double exponential fits of the fluorescence quenching provided two rates of loop conformational motion. We interpreted two rates of

conformational motion as a two-state binding mechanism where the initial binding state (B1) is the binding of the ligand that occurs in the extremities of the loops, and the secondary binding state (B2) is a conformational state that involves residues at the base of the loops and in the N-domain, and must occur before the uptake of ligand into the N-domain. Overall B1 rates were faster than B2 rates, with one exception in L11 where the rates were equal for the two binding states. Effects of fluorescence quenching for the two states of binding in the absence of TonB revealed faster rates of conformational motion and the rates for the two states were equal for most loops with three exceptions in loops L3, L4, and L5. L3 and L4 exhibited slower secondary rates of motion, and the reverse character was seen in L5.

Table 4.2 Effects of mutagenesis and fluorophore labeling on FeEnt uptake

	Binding[a]				Transport[b]				
	Unlabeled		FM–Labeled		Unlabeled		FM–Labeled		
Mutant–Loop	K_d (nM)	Capacity	K_d (nM)	Capacity	K_m (nM)	V_{max}	K_m (nM)	V_{max}	Nutrition[c]
++	1.53	110.76	2.23	111.67	1.22	124.2	2.18	99.69	13.5
T216C–L2	0.83	27.80	5.22	18.48	2.05	86.34	2.11	40.61	13.5
S271C–L3	2.12	97.71	4.04	90.94	1.45	93.46	2.24	67.01	13
A322C–L4	2.90	65.39	4.26	30.67	1.69	68.80	4.26	20.95	13
A383C–L5	6.75	91.90	4.71	20.65	2.96	50.41	6.16	35.64	13
S490C–L7	0.52	37.75	1.88	25.38	0.68	56.23	4.67	25.01	13
T550C–L8	1.68	53.16	3.32	30.77	2.20	125.7	2.91	29.45	13
A698C–L11	1.10	18.48	4.68	36.87	1.93	124.2	2.77	96.31	13.5

a. K_d (nM) and capacity [pmol ^{59}FeEnt bound $(10^9$ cells$)^{-1}$] of unlabeled loop mutants compared to FM-labeled mutants were measured by ^{59}FeEnt binding by analyzing triplicate mean values from two independent experiments by the 'bound versus total' equation in GRAFIT 6.0 (Erithacus Software).

b. K_m (nM) and V_{max} [pmol ^{59}FeEnt bound $(10^9$ cells$)^{-1}$min^{-1}] of unlabeled loop mutants compared to FM-labeled mutants were measured by ^{59}FeEnt binding by analyzing triplicate mean values from two independent experiments by the 'enzyme kinetics' equation in GRAFIT 6.0 (Erithacus Software).

c. Siderophore nutrition assay results for FeEnt growth diameter in millimeters were performed on all unlabeled single Cys mutants.

Unlabeled loop mutants compared to FM-labeled mutants were subjected to radioisotopic binding assay, which displayed overall decreases in binding affinity of FeEnt to FepA labeled mutants. These decreases in Kd were still in the nM range and compare to the wild type control of pits23, which has FepA with no Cys modification, and are therefore insignificant. However, decreases in binding capacity for FM-labeled mutants were a concern, and implied that the presence of the fluor label in the surface loops of FepA decreases the binding capacity at multiple sites in the surface loops. There were some exceptions in L11 and L3, which show no decrease and an increase in binding capacity, respectively. The most dramatic effect in binding capacity was seen for the mutant A383C–L5, which implied that L5 was very important for optimal binding of the ligand. Only minor differences were observed for the Km (nM) of unlabeled loop mutants compared to FM-labeled loop mutants. The Km for L4 and L5 were affected more than most other single Cys labeled sites, but the Km values are still in the low nM range. However, Vmax values decreased significantly in most of the loop sites, which indicated that the fluor label does affect the functionality of FepA uptake mechanism and likely the extent of conformation motion of the FepA loops and therefore the fluorescence changes.

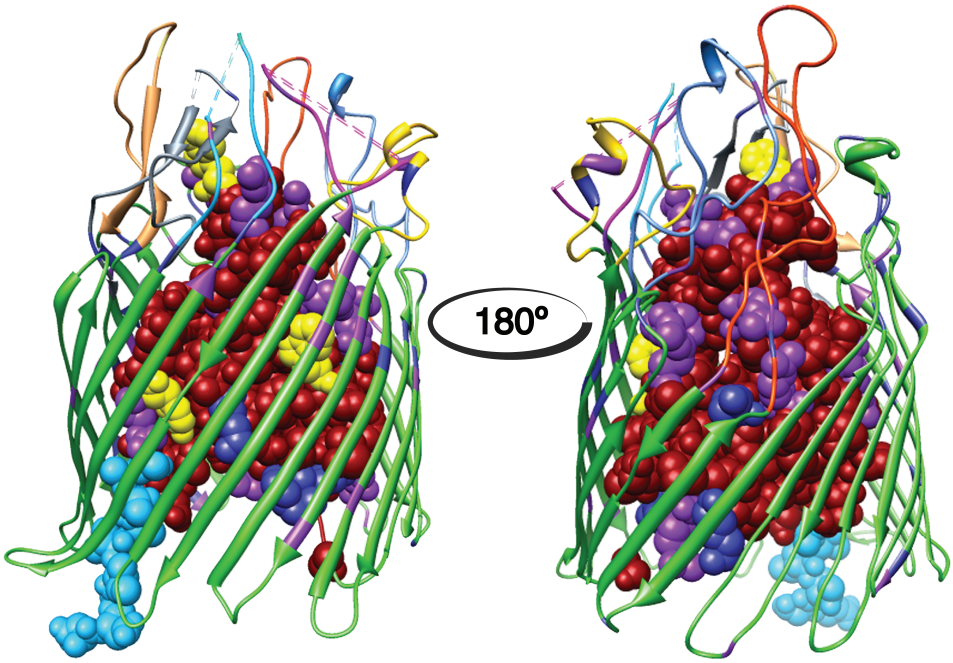

Figure 4.5 FepA crystal structure model.

The FepA crystal structure (180º rotation) with the B-barrel (green), N-domain (red space-filling) and the seven loops [L2 (cobalt blue), L3 (yellow), L4 (purple), L5 (cyan), L7 (grey), L8 (flesh), L11 (orange)] are highlighted in this study. The tonB box (cyan space-filling) is located on the periplasmic side of FepA directly below L7 and L8. There are only three aromatic residues in N-domain portion of FepA W101, W113, and Y133 (Y133 is located proximal to tonB box). However, numerous arginine (purple space-filling) and lysine (navy space-filling) basic residues line the N-domain interface with the B-barrel.

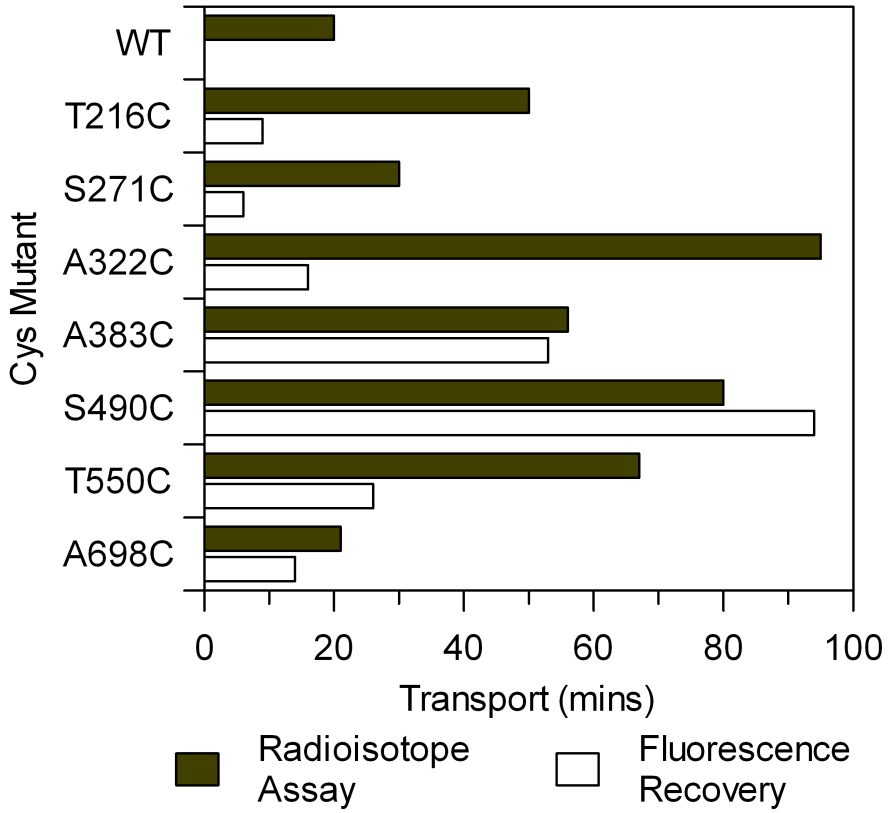

Figure 4.6 Comparison of FeEnt transport duration by two different methods.

The duration of transport in minutes was calculated from radioisotope Vmax transport rate (black bars) and fluorescence recovery rate (white bars) data of individual FepA Cys mutants. Each individual FepA Cys mutant was tested with 10nM FeEnt with cellular concentration of $5x10^7$ cells/mL in 1xMOPS buffer with 0.4% glucose. Although, pits23 (WT) plasmid containing FepA was the negative control during fluorescence

recovery analysis, it also represented unhindered FepA transport during radioisotopic transport assay.

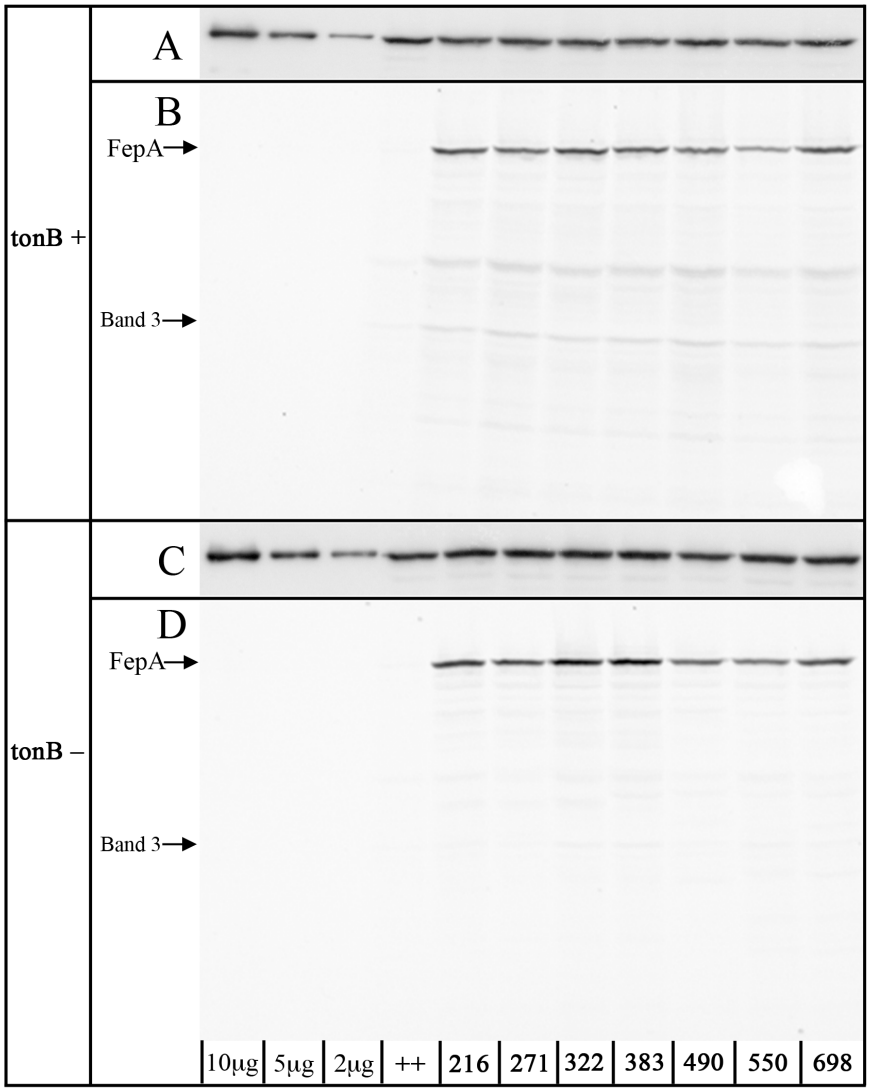

Figure 4.7 Individual Cys loop mutations: SDS-PAGE Gel and Immunoblot.

Individual strains were grown overnight in LB and subculture into MOPS minimal media. A. TonB+ I125-Protein A Immunoblot. B. TonB+ SDS-PAGE fluorescence gel scan. C. TonB- I125-Protein A Immunoblot D. TonB– SDS-PAGE fluorescence gel scan. The first three lanes of both runs contain purified FepA-His6 with amounts of 10µg, 5µg, and 2µg that were used for standardization amounts of µg of FepA.

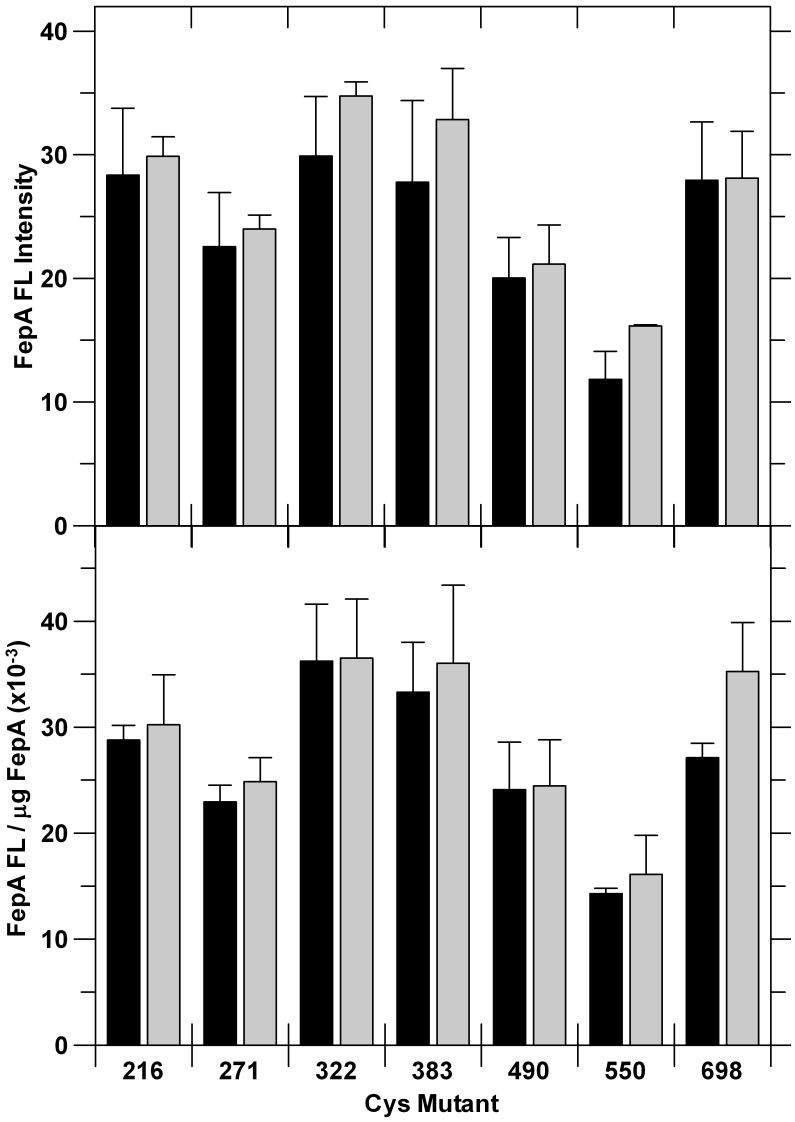

Figure 4.8 Evaluation of TonB-dependent conformation changes in FepA surface loops: Comparison of Cys fluoresceination in *tonB*+ and *tonB* cells.

Cys loop sites in FepA that were significantly labeled by FM were re-analyzed and compared in *tonB*+ (white bars) and *tonB*– (grey bars)

background cells. We incorporated the concentration of FepA (from anti-FepA ^{125}I-Protein A immunoblots) into calculations to compare the relative and absolute FM labeling levels.

Top panel. Relative levels of FM labeling in *tonB* + and *tonB* bacteria. Fluorescence images from SDS-PAGE gels of cell lysates were analyzed by IMAGEQUANT (Molecular Dynamics). Bars depict the mean FM labeling of FepA proteins relative to band 3 in OKN3 (white) and OKN13 (grey; mean of two experiments, with associated standard error). FepA proteins were equally fluoresceinated in the *tonB* strain (Fig. 4.7).

Bottom panel. Absolute levels of FM-labeling in *tonB*+ and *tonB* strains. The extent of Cys residue labeling was corrected for the expression level of each mutant FepA protein, to yield the absolute labeling level (fluorescence intensity/μg FepA). The correction eliminated the subtle differences in labeling between *tonB*+ and *tonB* cells seen in the top panel.

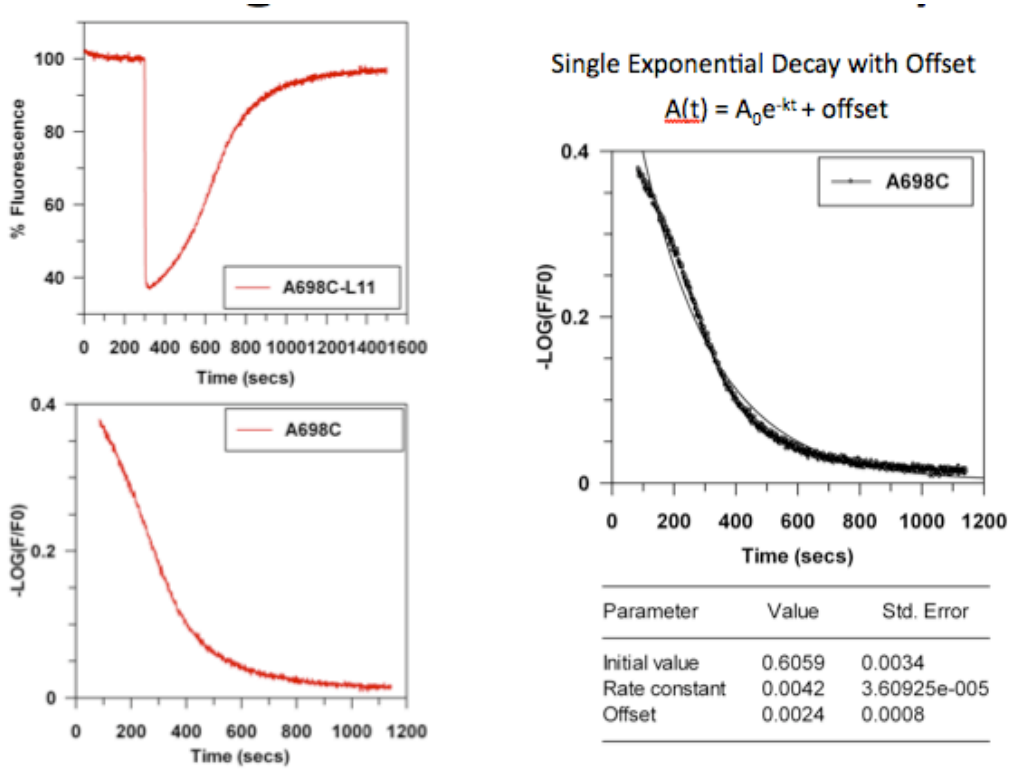

Figure 4.9 Fluorescence recovery curve single exponential fitting analysis

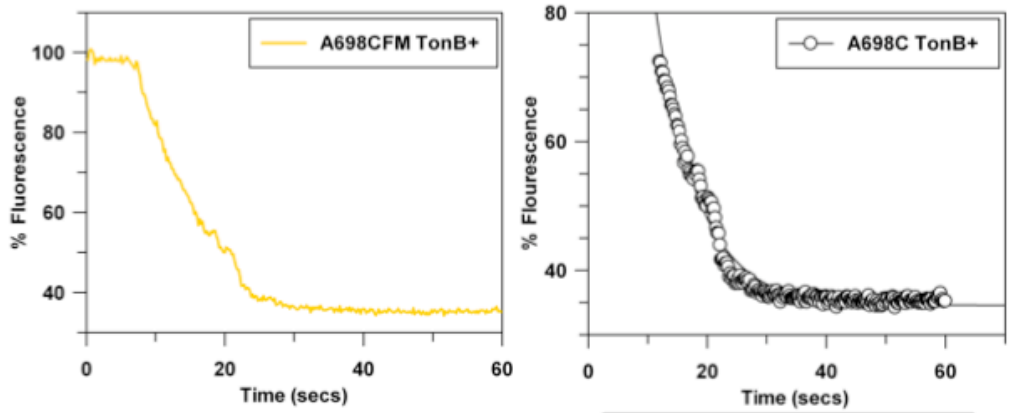

Double Exponential Decay with Offset:

$A(t) = A_{0(1)}e^{-k1t} + A_{0(2)}e^{-k2t} + \text{offset}$

Parameter	Value	Std. Error
Initial value 1	128.7684	13.8745
Rate constant 1	0.1400	0.0076
Initial value 2	95.9580	13.2238
Rate constant 2	0.1412	0.0077
Offset	34.5551	0.1378

Figure 4.10 Fluorescence quenching curve double exponential fitting analysis

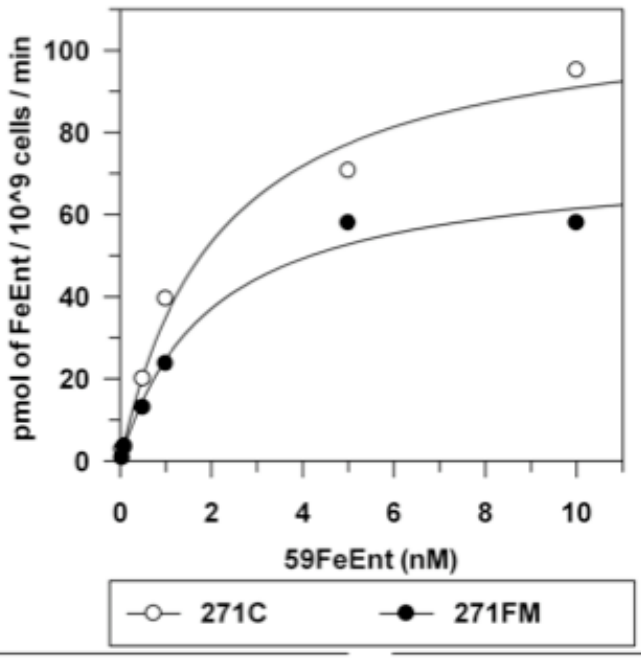

Parameter	Value	Std. Error
Vmax	110.5598	7.9684
Km	2.1576	0.4793

Parameter	Value	Std. Error
Vmax	73.5723	5.4952
Km	1.9738	0.4645

Figure 4.11 Radioactive transport fitting of unlabeled vs. FM-labeled S271C.

The above graphs depict an example of fitting the ^{59}FeEnt transport characterizing FepA with a single Cys mutation at S271C under unlabeled (white circles) and FM-labeled (black circles) conditions to collect kinetic parameters Km (nM) and Vmax (pmol / 10^9 cells / min).

Discussion

Fluorescence quenching rates reveal a two-state binding mechanism in the FepA surface loops

In vivo fluorescence spectroscopy of individually labeled FepA loops indicated specific loop conformational changes during FeEnt uptake. ^{59}FeEnt binding and transport results revealed global changes due to individual mutations in FepA surface loops modified with attached fluorophores. Nevertheless, spectroscopic observations of fluorescence changes in individual FepA loops allowed visualization of conformational changes in specific loops as well as kinetic rates of ligand uptake that reveal local mechanistic trends in the FepA surface loops during FeEnt uptake. Fluorescence quenching time course data fitted to the double exponential decay equation displayed two separate rate constants, which were interpreted as B1 and B2 rates of binding. The two binding rates agreed with previous alanine scanning of aromatic residues in the surface loops of FepA that proposed the two-state binding model (49). The model postulated an initial binding state (B1) that occurred faster than the secondary binding state (B2), which participates in the uptake of the ligand with the N-domain mechanism (49). These data verified the two-

state binding mechanism and refined the time frame for ligand binding and uptake that was previously reported (Tables 4.1, 4.2).

Based on fluorescence changes of individual loops, we separated the seven loop mutants (L2, L3, L4, L5, L7, L8, L11) into two groups to characterize the behavior of individual loop conformational motion during ligand uptake and binding. Group A (L2, L3, L11) exhibited large extents of quenching with fast recovery rates, whereas Group B (L4, L5, L7, L8) exhibited slow recovery rates and small extents of quenching with an exception for S490C–L7, which resembled Group A quenching extents. Furthermore, sequentially decreasing rates of recovery were observed from Group A side of the FepA surface loop domain to the Group B loop side (Table 4.2). However, the consistently faster B1 rate of L2 is similar to B1 rates of Group B loops that are proximal, which may suggest a shared role during the initial stage of ligand binding. For example, Group A loops are adjacent to one another and quench to about the same extent, but exhibit differential B1 quenching character, whereas L2 quenched 6 times faster than either L3 or L11 during B1. Moreover, Group A quenchers displayed very similar B2 uptake half-lives, which indicated that their roles during the second stage of ligand binding are related. The slower B2 rates imply that Group A loops are needed to maintain ligand

contact that would be necessary for optimal uptake into the N-domain. Interestingly, Group B all displayed similar B1 half-life rates with gradient distribution speeds of L4 > L5 > L8, with almost reciprocal differences during B2 of L8 > L5 > L4, which provided further evidence for the importance of individual loops during a sequential ligand uptake mechanism with an emphasis on Group B loops during B2 phase of binding and transport.

The fluorescence recovery phase represents the depletion of FeEnt from the surrounding culture (35) and the average return of the loops to unbound conformation. Figure 2 clearly demonstrates fluorescence changes of individual loops where rates of recovery exhibited sequential times of recovery moving from Group A side of FepA to the Group B side, with faster rates for Group A loops and slower rates for Group B loops. The slowest conformational recovery occurred in loops that were proximal to L7, whereas L7 displayed the slowest rate of fluorescence recovery. Differences in the duration of transport were calculated to compare the two different methods of measuring transport function, fluorescence recovery and ^{59}FeEnt transport (Fig. 4.6). The marked differences in duration of transport between the radioisotope transport and fluorescence recovery methods for Group A loops appeared to highlight the ability of

fluorescence spectroscopy to measure the changes of individual loops as oppose to measurements in the global changes of the FepA loops from radioisotope transport measurements. On the contrary, Group B duration of transport between the two transport assays was very similar. Therefore, shorter transport duration times for Group A mutants during the fluorescence recovery measurements revealed that some loops, such as L2 and L3, relinquish contribution for ligand uptake before the actual uptake of ligand in the FepA loops come to completion. These results further indicated that the rate-limiting step in FepA loop binding reaction resides within Group B loops above the postulated tonB-box sequence of the FepA N-terminal domain.

Effects of loop motion in the absence of the TonB

Fluorescence intensity changes in FepA were known to be TonB dependent (35), therefore we used fluorescence quenching to study the binding of FeEnt for the various FepA loops in tonB+ and tonB– background cells. Previous studies explored fluoresceination accessibility in FepA that provided evidence for TonB dependent conformations within the N-domain of FepA, where the N-domain residue G54C was accessible in the presence of TonB but inaccessible in tonB– cells (37). If the N-

domain and surface loops cooperate during FeEnt binding and uptake, then FepA surface loops would exhibit distinct conformational and kinetic characteristics between tonB+ and tonB– cells. Fluorescence results of mutants in the tonB+ background revealed slower quenching rates in B2, which implied slower positioning of the ligand during preparation for transport through the globular N-domain in the presence of the postulated IM energy transducer TonB. Furthermore, no change in the rates between B1 and B2 were observed in tonB– cells, where the B2 state was identical to the B1 state, implying that the mechanism of ligand entry into the N-domain was altered compared to tonB+ cells. Whereas, during the B1 binding phase the loops ensconced the ligand, but could not transition conformational states to move the ligand into position with the help of the N-domain loops during the B2 phase of binding. For most of the loop sites in the tonB– cells, rates of quenching were much faster during B2 compared to B2 rates in the tonB+ background. There was one exception for A322C-L4 in tonB– cells, where fluorescence quenching half-life of 11.85 seconds was observed, which was consistent and also displayed significant defects for ^{59}FeEnt transport. Interestingly, T550C–L8 fluorescence quenching remained relatively constant between both tonB background cells and exhibited severely hindered binding and transport by

the fluor attachment, which most likely prevented L8 from fully participating in the uptake of the ligand. The overall faster quenching rates during the B2 phase for all loops in tonB– cells implies that an order mechanism of FeEnt entry into the N-domain occurs in the FepA loops when TonB is present.

Possible ligand entry into the N-domain on Group B side of FepA

Considering the mechanism of metal ligand binding, if ligand uptake is in someway significantly hindered by the Cys mutation or fluor attachment, then a pathway for ligand entry must exist relative to the modified loop domain. The sensitivity of measuring fluorescence changes in the FepA loops allowed the elucidation of loop roles for ligand uptake for Group A (L2, L3, L11) loops, which were ancillary to the central role of Group B (L4, L5, L7, L8) loops in the uptake mechanism. Coincidentally, ligand entry occurs at the base of Group B loops, which reside directly above the FepA N-terminal TonB box in the crystal structure (Fig. 4.5). Ideally, once the ligand is situated in the B2 state, the postulated mechanical force induced by the TonB complex could activate N-domain conformational changes required for ligand passage into the periplasmic space. If such a mechanical force were to act on the N-domain, no matter

the direction, the ligand would be ideally situated at the base of Group B loops for N-domain entry. Furthermore, fluorescence quenching in the tonB– background revealed that loop conformational changes appeared partially dependent on the N-domain mechanism (Fig. 4.4). Therefore, if the extent of loop motion is dependent on TonB action of the N-domain, then the possibility exists for a 'holding area' at the base of Group B loops. Interestingly, Group B loops all have unresolved segments seen in the FepA crystal structure, which imply flexibility and likely exhibit significant extents of motion. As expected, any mutation located within the postulated FepA binding vestibule displayed severe difficulties during ligand uptake and displayed no fluorescence changes. S275C–L3 was likely positioned in the proposed B2 site of the FepA vestibule, which prevented the proper conformational conditions for ligand binding and uptake.

Radioisotopic ^{59}FeEnt binding and transport data were measured and compared to pits23 with no Cys mutations, results indicated that the presence of the fluorophore attachment to loop Cys sites trammeled the uptake of the ligand through FepA for all loops to different extents. Likewise, slower rates of fluorescence changes for individual loop reflected the decreased FeEnt binding and transport ability of FepA. Kinetics of L2, L3, and L11 FepA mutants were similar to wild type levels

of binding and transport, which suggested that all three loops of Group A participated in at least the initial binding event of FeEnt and do not hinder the ligand uptake process into the N-domain (Figs. 4.3, 4.4). Furthermore, fitting fluorescence quenching data of Group A loops, showed good agreement to single exponential fitting of time course curves, which indicated that Group A loops exhibited the singular binding function. However, Group B loops did not agree with single exponential fitting, they displayed a biphasic character of rates and were applied to double exponential fits of the time course curves. Hence, to properly compare Group A and Group B rates of quenching we fitted all fluorescence quenching time course results to double exponential fits, which simply displayed equal Group A B1 and B2 rates. The slower fluorescence quenching and recovery results of Group B loops L4, L5, L7, and L8 indicated that these loops played a pivotal role in the B2 phase, hence the loop conformational states prior to FeEnt uptake by N-domain mechanism.

The Kd of each binding event for L2 display a consistent initial binding with a much slower secondary binding. The comparison in the absence of tonB displayed the distinct effect in the loops when TonB does not initiate a conformational change in the FepA N-domain, which appears to permeate to the FepA surface loops. The presence of the fluor label on

L2 displayed hindrance effects during the binding stage, but displayed no difference during transport of the ligand. The transport duration from fluorescence recovery was much faster when compared to the radioisotope data for L2, which highlights the ability of fluorescence spectroscopy to analyze individual loop function.

Binding kinetics for L3 appear to be much slower than even L2 but still display a slow B1 rate compared to B2 rate. The comparison of tonB absence background displays similar trends between binding ability. Furthermore, the presence of the fluor label does not seem to cause significant perturbations in for either binding or transport. The fluorescence recovery again illustrates the ability to visualize individual loops, but L3 duration of transport appears to still affect global conformation changes in the surface loops.

The L4 binding kinetics display the overall trend of a faster B1 rate with a slower B2 rate. The dramatic difference for duration of transport of L4 between radioisotope and fluorescence recovery data highlight the dependency of global surface loop conformation on L4, which the fluor attachment clearly hinders. The absence of tonB exacerbates the secondary binding ability of L4 with the slowest of all loop rates at 11.85

for B2. These results provide further evidence for TonB dependent conformations in the surface loops.

The binding kinetics of L5 display similar trends, but in the absence of tonB the rates of B1 and B2 reverse in comparison to tonB+ background. This result in context of binding function from radioisotope data suggest that L5 function is indeed hindered by fluor label, and the slow recovery rate emphasizes this hindrance by the fluor label. The duration of transport for L5 is equal in either method, which seems to define L5 as a valuable contributor to the global conformation changes necessary for optimal ligand binding.

Previous study by Scott et al. (31) was able to observe motion in L7, cross-linking L7 to other proximal OM proteins. The binding kinetics displayed no difference between B1 and B2, and no difference between B1 and B2, but faster rates in the absence of tonB. Furthermore, radioisotope binding and transport data display severe effects with or without the fluorophore attachment. The duration of transport between the two methods is almost equal, with L7 displaying the weakest ability to bind and transport the ligand. These data display for the first time L7 ability to play a pivotal role in the uptake of FeEnt from the initial binding stage to the uptake by the N-domain, which is dependent on the presence of tonB.

Annamalai et al. previously demonstrated that aromatic residues of L7 (Y478, Y495) were crucial to the uptake reaction with only minor contributions during binding events. Therefore, results from the S490C–L7 mutation were as expected, however, other mutations were designed in L7 (S470C, S482C) that displayed no change in fluorescence. Analysis of all L7 sites displayed significant binding and transport defects when fluorophores were attached with fluorescence changes only from mutations in the apical portion of the loop.

Previous studies indicated L8 as a crucial loop for both optimal binding and uptake of the ligand to occur. The binding kinetics of L8 displays similar trends where B1 is faster than B2. However, the absence of tonB reveals that B1 and B2 rates becomes equal, which indicated that L8 loop conformational is dependent on presence of TonB action on the N-domain. The transport of 59FeEnt shows a difference in Vmax, but not the affinity of the ligand. Moreover, the duration of transport reveals that although fluorescence recovery displays relatively efficient transport, the global surface loop conformations are effected by L8 modification.

We designed two different mutations in L10 at G640 and T648 and subjected them to the same labeling procedure, neither displayed

fluorescence changes due to either an inactive role in transport or significant defects due to the fluor attachment to the loop site.

Although the binding function of L11 seems to be hindered, the transport function does not appear to be hindered by the attachment of the fluor label. The binding kinetics from fluorescence spectroscopy reveals interesting B1 and B2 character, where both are very similar for L11. However, in the absence of tonB the binding kinetics rates become much faster, which indicate that both binding events end much earlier without TonB induced conformational changes in the N-domain. This is also evident from transport duration, where L11 is unique in that both methods display relatively equal durations of transport. These results indicate that L11 does in fact participate in the binding event; however even with the fluor attachment the role of L11 remains in the binding event stage and does not perturb the uptake event of the ligand into the N-domain.

The former uncertainty of TonB dependent conformational states within the FepA surface loops could be attributed to an inability of precisely characterizing individual loop conformational events during FeEnt binding and uptake in live cells by previous methods. The novelty of fluorescence spectroscopy in live cells has been the precise characterization of individual loop conformational motion and kinetic rates

during FeEnt uptake. These results provide valuable evidence for TonB dependent changes in the FepA surface loops that likely reverberates throughout FepA by the simple association of TonB. Future studies of the FepA mechanism will involve the design of constructs to remove energy from the TonB system, such ExbB, D deletions, that could provide further information about the movement of the N-domain and energy transduction between membranes of Gram (–) cells.

Chapter 5 : Confocal imaging of TonB-GFP localization within live cells

Background

Small-molecule nutrients can enter the cell through open pores in the OM. However, larger nutrients such as metal complexes, which are scarce in the extracellular milieu, must be actively transported via high affinity OM receptors that utilize energy-coupled reaction mechanisms. OM transporters contain closed channels and bind metal complexes, heme, colicins and phage with high affinity active transport of these metal complexes and toxins requires energy from the proton motive force (pmf), which involves the IM protein TonB complex (39,98,99). The TonB complex is composed of multiple subunits (ExbB, ExbD, TonB) that reside in the periplasmic space, inner membrane and the cytoplasm (51). The transmembrane protein ExbB is proposed to form the core of the complex on which ExbD and TonB are formed and added to complete the TonB-ExbB-ExbD complex (100). Using liquid bead ion desorption mass spectrometry Pramanik et al. (101) observed the complex of six ExbB subunits and ExbB-ExbD with a ratio of 6:1, where the ExbB subcomplex must form the core complex with ExbD before TonB is recruited. However,

a previous study by Higgs et al. used a radiolabel method that indicated the ExB:ExbD:TonB complex ratio 7:2:1 in cell lysates(102).

Numerous studies provide evidence that TonB associates with the N-terminus of OM transporters, where TonB-association combined with a proposed mechanical force is transduced by the pmf-fueled TonB-ExbD-ExbB complex (1,21,51,103). Post-uptake binding experiments measured uptake of ^{59}FeEnt through FepA and estimated a 35:1 FepA to TonB ratio, which also revealed that not all FepA are functional at one time (104). Therefore, the action of TonB is likely coupled to the rate-determent step in the transport process for all OM transporters. However, the mechanism of how TonB complex transduces energy to the OM is still undetermined. Kaserer et al. discovered that TonB not only has an affinity to N-domain OM receptors but the association does not require a TonB-box and LysM binding motif indicated the persistent association of TonB with peptidoglycan (51). Kaserer et al. (51) TonB-peptidoglycan surveillance model highlighted surprising new dimensions of the TonB functional mechanism, and the creation TonB-GFP fusion protein provided an opportunity to visualize the distribution of TonB-GFP within the IM of living cells. Plasmids (pGT) containing TonB-GFP fusion protein were purified and transformed into *E.coli* cells containing pits23 plasmid expressing

FepAS271C. The cells containing the two different plasmids were treated with Alexafluor Maleimide dyes and prepared for confocal fluorescence microscopy (see experimental procedures). Confocal fluorescence microscopy with multiple photon detectors allowed visualization of TonB and FepAS271C-AM distribution in live cells that revealed unique distributions of TonB in the IM of the *E. coli* cells.

Results

Design of constructs, selection of fluorescence dyes, and confocal fluorescence microscopy imaging

We analyzed OKN3 cells containing both TonB-GFP (pGT) and S271C (pits23) plasmids then labeled the cells with Alexafluor dyes (see experimental methods). AlexaFluor fluorescence dyes (Invitrogen, Carlsbad, CA) with absorption maxima either 555nm or 670nm were used to maintain clear separation of absorption spectra from the GFP excitation and emission spectra during multiple photon confocal microscopy imaging. We transformed plasmid-expressing LacY-GFP into OKN3 cells containing plasmid pits23 expressing S271C (pLp271) and labeled Cys sites of FepA-S271C in cells with Alexafluor dyes. Images of labeled cells were captured with confocal fluorescence microscopy by the Olympus

FluoView FV1000 (Olympus America Inc.; Center Valley, PA) or Zeiss LSM 7 MS (Carl Zeiss LLC; New York, NY) with two different photon detector channels to detect fluorescence emission from GFP and Alexafluor 555 simultaneously. Microscopy 100X objectives were used with fluorescence detection by multiple photons or the imaging of unlabeled cells with differential interference contrast (DIC) microscopy.

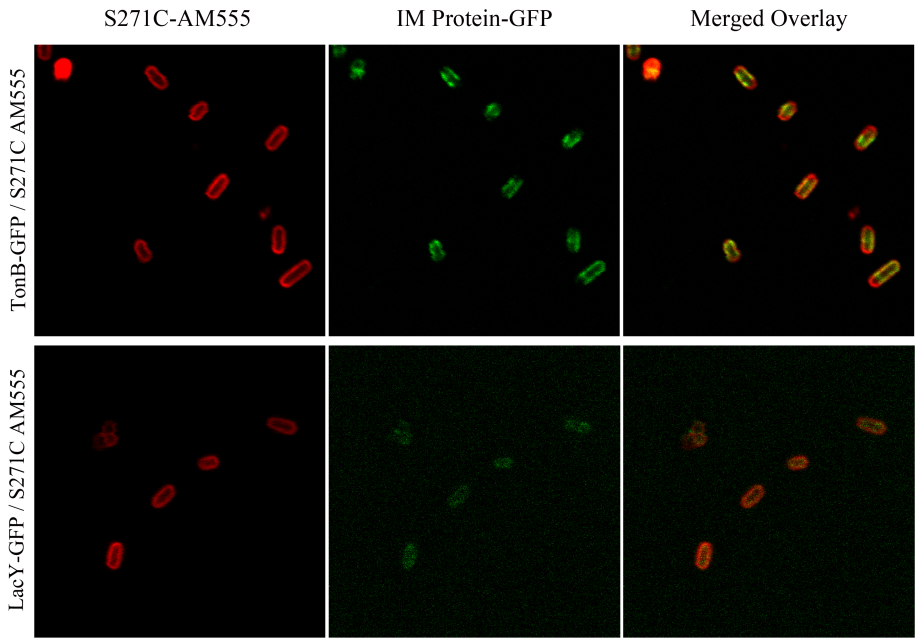

Figure 5.1 Inner membrane-GFP fusion proteins with AM-labeled FepA.

Cells were immobilized on poly-lysine glass slides and imaged in confocal fluorescence microscopes with multiple photon attachments. Labeled Cys sites at 271 in FepA allowed visualization of the distribution of FepA inside cells (left set of panels). The hybrid IM proteins that both were attached to GFP were visualized in a separate channel from Alexafluor 555 (center panels). The overlay of these two channels combined the fluorescence from FepA-S271C-AM555 and IM GFP hybrid proteins resulting in the

relative distribution of FepA in the OM compared to LacY or TonB in the IM of *E. coli* (right panels).

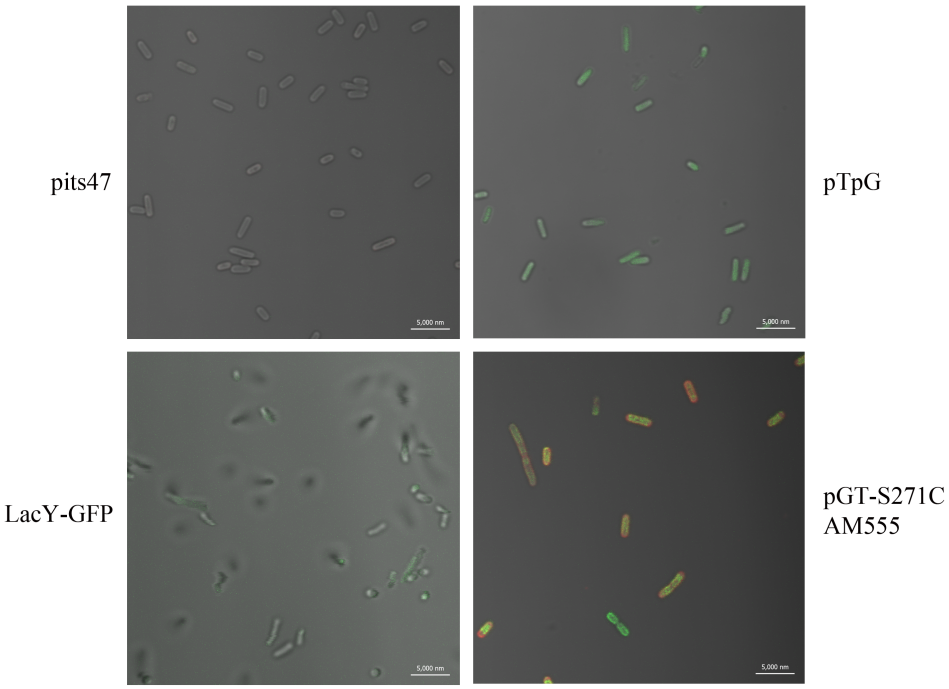

Figure 5.2 Confocal microscopy fluorescence: Intensity comparison. We labeled pits47 (top left), pTpG (top right), and LacY-GFP (bottom left) with AlexaFluor dyes and compared images to pGT-S271C-AM555 (bottom right) with identical confocal imaging settings in the Zeiss LSM 7 MS (Carl Zeiss LLC; New York, NY) to qualitatively compared labeling intensities of cells.

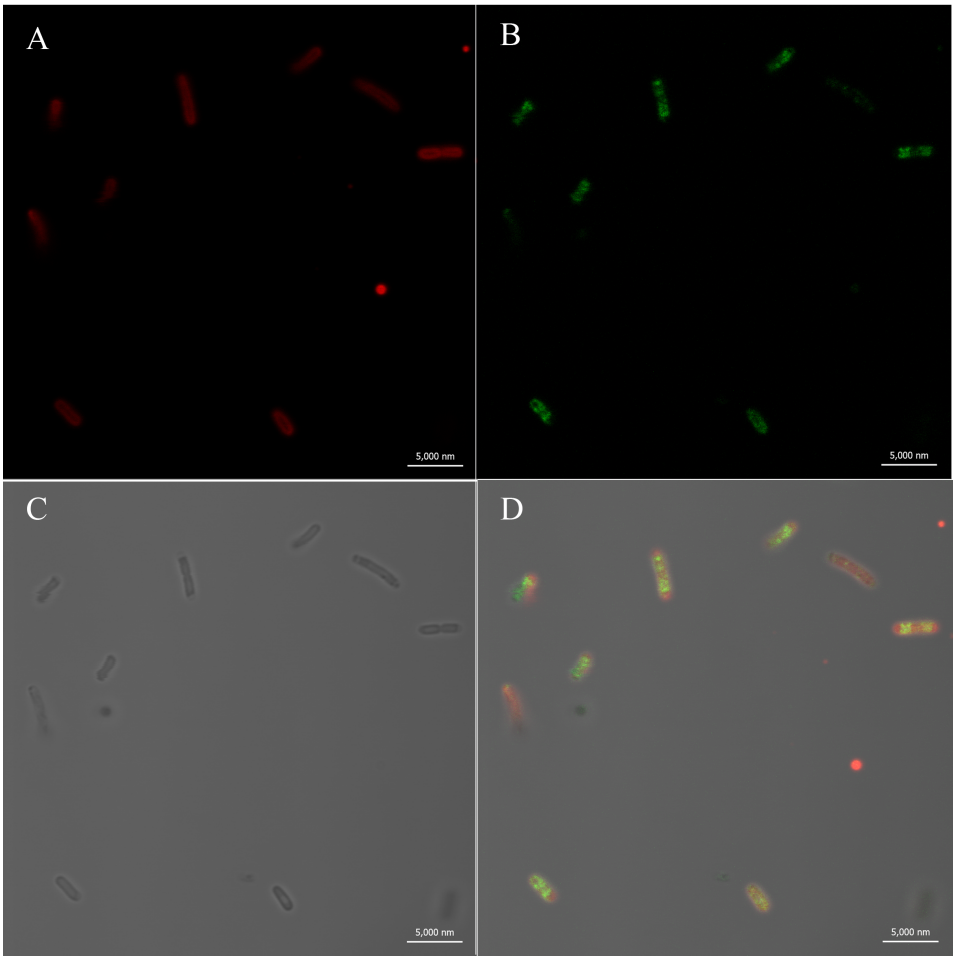

Figure 5.3 Confocal imaging of TonB localization during cell division. Cells expressing AM555-labeled FepA-S271C (A) and TonB-GFP hybrid proteins (B) were imaged by Olympus FV1000 with multiple photons displayed unique distribution of TonB-GFP compared to FepA-S271C in the poles of dividing cells (D). These cells with also imaged simultaneously with DIC (C) to observe the real-time distribution of fluorescence from two different fluorescence probes inside living cells.

Discussion

Localization of TonB appeared to be dependent on the state of cell division, where a division of TonB-GFP population into equal parts within each daughter cell was observed (Fig. 5.3 B & D). Two distinct loci were observed in dividing cells of figure 5.3.D (in the upper right quadrant), which indicated, during cell division, the population of TonB-GFP is somehow conserved in equal parts of each daughter cell. The faint fluorescence response from the even distribution of LacY-GFP in the IM was observed (figure 5.1 & 5.2), which emphasized the uniqueness of the TonB-GFP distribution within the IM of E. coli. These results could benefit from the understanding and further characterization of other IM protein complexes such as other IM permease. Although, confocal fluorescence microscopy was not powerful enough to differentiate between the two membranes of *E. coli*, the use of two different fluorophore labeled proteins allowed the simultaneous observation of TonB-GFP distribution in the IM and FepA in the OM within live cells. The isolation of dividing cells using sucrose gradients (105) and new methods of arresting cell division (106) could reveal further information about the distribution character and function of TonB-GFP during cellular growth. Hence, as the mechanistic role of TonB is further characterized, the distribution of the IM TonB

protein complex could reveal new insights into how bacteria coordinate the need for IM energy transducing systems during cell division.

Chapter 6 : Summary of research and future directions

Mechanistic insights of FepA transport attained from fluorescence probes in bacterial membranes highlight the difficulty of investigating membrane transport mechanisms in live cells. Nevertheless, detection of fluorophore probes with fluorescence spectroscopy provided novel precise measurements of fluorescence changes that revealed unique perspectives of FepA surface loop conformational states during various conditions. Analysis of fluorescence changes of labeled sites in the FepA surface loops provided further evidence of the FepA surface loops dynamic conformational motion in live cells, which allowed characterization of FepA loop roles during FeEnt binding and transport.

Probing the FepA with fluoresceination in vivo with over 35 genetically modified single cysteine sites provided a blue print to test multiple interactions within the FepA transport mechanism. Analysis of conformational loop motion from fluorescence spectroscopy data revealed that high–affinity binding in FepA surface loops is more ordered than previously anticipated and also occurs independent of TonB within the second timescale. The FepA loops position FeEnt in a holding area and await TonB-induced conformational changes within the N-domain for active transport of FeEnt into the periplasm. We designed mutants in eight

(L2, L3, L4, L5, L7, L8, L10, L11) of the nine active FepA surface loops and measured fluorescence responses from all loops except L10. Although each loop participates in FeEnt uptake, these results were able to identify roles of each individual loop during the ligand uptake reaction (Table 6.1).

Table 6.1 Proposed roles for individual FepA surface loops during FeEnt uptake

Cys Mutation–Loop	Group[a]	Loop Basic & Aromatic Residues[b]	Loop Role during FeEnt Uptake[c]
T216C–L2	A	2:B 2:A	Located at Group A-B interface; likely participates in initial binding and ligand positioning
S271C–L3	A	2:B 3:A	Involved in Initial binding step; doesn't appear to participate in secondary binding
A322C–L4	B	2:B 0:A	Positioning ligand in binding vestibule
A383C–L5	B	3:B 1:A	Positioning ligand in binding vestibule
S490C–L7	B	2:B 5:A	Maintains constant ligand contact; evenly spaced Tyrosine residues likely act as guides for ligand from outer loops into N-domain
T550C–L8	B	0:B 3:A	Loop role is to assist L7 (aromatic sites at base of loop) in maintaining ligand position during uptake
T648C–L10	–	5:B 2:A	–
A698C–L11	A	2:B 5:A	Largest loop; loop maintains constant contact with ligand during binding and possibly uptake

a. Loops were separated into two-groups based on fluorescence changes due to conformational motion of loops reacting with FeEnt

b. Number of basic (B) and aromatic (A) residues contained in each individual FepA loop that could contribute to uptake of the acidic-aromatic ligand FeEnt

c. Proposed role of loop contribution to the FeEnt uptake reaction based on fluorescence spectroscopy and 59FeEnt radioisotopic binding and transport results

Annamalai et al. described the effects of numerous aromatic and basic substitutions in the FepA surface domain (49). Although we designed loop mutations with these aromatic sites in mind, a possibility for fluorescence changes could be due to alterations in the environment caused by the attached fluor and not necessarily the conformational motion of individual loops. The likelihood of significant alterations in FepA functional conformation due to the fluor is small for most loops, and this is especially noticeable from ^{59}FeEnt functional assay, which displayed small effects in the fluor attachment as opposed to the significant functional effects in alanine scanning mutagenesis study of aromatic sites (49).

Newton et al. (1999) described the binding and transport effects of loop deletions, however deleting significant portions of FepA skewed conclusions of loops that provided support roles, but did indicate important loops proximal to L7. The unobtrusive aspects of fluorescence probes used in this dissertation were specifically designed to maintain native conformation and function in FepA to obtain results that were biologically relevant. Analysis of fluorescence changes in the surface loops displayed significant evidence that suggested the loop uptake mechanism ends with loops proximal to L7. These new insights into loop contribution to FeEnt transport combined with recent results from Newton et al. (2010) suggest

the N-domain transport of FeEnt contains multiple steps, with the translocation through the N-domain likely the slowest step in the reaction.

The novel approach of utilizing site-directed single Cys mutagenesis and fluorescence probes in live cells, although tedious and time consuming, provided powerful biologically-relevant results that revealed further evidence of the FepA binding and transport mechanism. Although, some evidence existed for a possible FepA N-domain pathway for FeEnt, analysis of loop fluorescence changes clearly identified a ligand entry point into the N-domain at the base of Group B loops. However, a pathway for colicin entry into the cell is still undefined. The contributions from the simple binding of TonB must be further explored in vivo. Therefore, future studies should involve the continued use of fluorescence probes in conjunction with crosslinking of multiple Cys sites in the N-domain that may inhibit the uptake of FeEnt or ColB and to obtain further biologically relevant evidence for FepA transport mechanism. Further experiments utilizing the crosslinking of the N-domain could reveal the entry mechanism for FeEnt and ColB.

References

1. James, K. J., Hancock, M. A., Moreau, V., Molina, F., and Coulton, J. W. (2008) *Protein Sci* **17**, 1679-1688

2. Devanathan, S., and Postle, K. (2007) *Mol Microbiol* **65**, 441-453

3. Levy, S. B., and Marshall, B. (2004) *Nat Med* **10**, S122-129

4. Bush, K., Courvalin, P., Dantas, G., Davies, J., Eisenstein, B., Huovinen, P., Jacoby, G. A., Kishony, R., Kreiswirth, B. N., Kutter, E., Lerner, S. A., Levy, S., Lewis, K., Lomovskaya, O., Miller, J. H., Mobashery, S., Piddock, L. J., Projan, S., Thomas, C. M., Tomasz, A., Tulkens, P. M., Walsh, T. R., Watson, J. D., Witkowski, J., Witte, W., Wright, G., Yeh, P., and Zgurskaya, H. I. *Nat Rev Microbiol* **9**, 894-896

5. Areschoug, T., and Gordon, S. (2009) *Cell Microbiol* **11**, 1160-1169

6. Raymond, K. N., Dertz, E. A., and Kim, S. S. (2003) *Proc Natl Acad Sci U S A* **100**, 3584-3588

7. Neilands, J. B. (1983) *Adv Inorg Biochem* **5**, 137-166

8. Vernon, L. P. (1968) *Bacteriol Rev* **32**, 243-261

9. Philpott, C. C., Klausner, R. D., and Rouault, T. A. (1994) *Proc Natl Acad Sci U S A* **91**, 7321-7325

10. Gawron, O., Waheed, A., Glaid, A. J., 3rd, and Jaklitsch, A. (1974) *Biochem J* **139**, 709-714

11. Klein, J. S., and Lewinson, O. *Metallomics* **3**, 1098-1108

12. Leong, J., and Neilands, J. B. (1976) *J Bacteriol* **126**, 823-830

13. Neilands, J. B. (1981) *Annu Rev Biochem* **50**, 715-731

14. Neilands, J. B. (1976) *Ciba Found Symp*, 107-124

15. Bagg, A., and Neilands, J. B. (1987) *Biochemistry* **26**, 5471-5477

16. Tufano, T. P., Pecoraro, V. L., and Raymond, K. N. (1981) *Biochim Biophys Acta* **668**, 420-428

17. Guterman, S. K., Morris, P. M., and Tannenberg, W. J. (1978) *Gen Pharmacol* **9**, 123-127

18. Nikaido, H. (1994) *J Biol Chem* **269**, 3905-3908

19. Braun, V., Hantke, K., and Koster, W. (1998) *Met Ions Biol Syst* **35**, 67-145

20. Braun, V. (1998) *Science* **282**, 2202-2203

21. Schauer, K., Rodionov, D. A., and de Reuse, H. (2008) *Trends Biochem Sci* **33**, 330-338

22. Braun, V., Mahren, S., and Sauter, A. (2006) *Biometals* **19**, 103-113

23. Braun, V., and Endriss, F. (2007) *Biometals* **20**, 219-231

24. Postle, K., and Larsen, R. A. (2007) *Biometals* **20**, 453-465

25. Letain, T. E., and Postle, K. (1997) *Mol Microbiol* **24**, 271-283

26. Payne, M. A., Igo, J. D., Cao, Z., Foster, S. B., Newton, S. M., and Klebba, P. E. (1997) *J Biol Chem* **272**, 21950-21955

27. Buchanan, S. K., Smith, B. S., Venkatramani, L., Xia, D., Esser, L., Palnitkar, M., Chakraborty, R., van der Helm, D., and Deisenhofer, J. (1999) *Nat Struct Biol* **6**, 56-63

28. Klebba, P. E., Rutz, J. M., Liu, J., and Murphy, C. K. (1993) *J Bioenerg Biomembr* **25**, 603-611

29. Cao, Z., Qi, Z., Sprencel, C., Newton, S. M., and Klebba, P. E. (2000) *Mol Microbiol* **37**, 1306-1317

30. Wiener, M. C. (2005) *Curr Opin Struct Biol* **15**, 394-400

31. Scott, D. C., Newton, S. M., and Klebba, P. E. (2002) *J Bacteriol* **184**, 4906-4911

32. Rabsch, W., Ma, L., Wiley, G., Najar, F. Z., Kaserer, W., Schuerch, D. W., Klebba, J. E., Roe, B. A., Laverde Gomez, J. A., Schallmey, M., Newton, S. M., and Klebba, P. E. (2007) *J Bacteriol* **189**, 5658-5674

33. Postle, K. (1990) *Mol Microbiol* **4**, 2019-2025

34. Di Girolamo, P. M., and Bradbeer, C. (1971) *J Bacteriol* **106**, 745-750

35. Cao, Z., Warfel, P., Newton, S. M., and Klebba, P. E. (2003) *J Biol Chem* **278**, 1022-1028

36. Newton, S. M., Igo, J. D., Scott, D. C., and Klebba, P. E. (1999) *Mol Microbiol* **32**, 1153-1165

37. Ma, L., Kaserer, W., Annamalai, R., Scott, D. C., Jin, B., Jiang, X., Xiao, Q., Maymani, H., Massis, L. M., Ferreira, L. C., Newton, S. M., and Klebba, P. E. (2007) *J Biol Chem* **282**, 397-406

38. Mahoney, A. M., Stimpson, C. L., Scott, K. L., and Hampson, N. B. (2007) *Respir Care* **52**, 1741-1743

39. Cao, Z., and Klebba, P. E. (2002) *Biochimie* **84**, 399-412

40. Smallwood, C. R., Marco, A. G., Xiao, Q., Trinh, V., Newton, S. M., and Klebba, P. E. (2009) *Mol Microbiol*

41. Liu, J., Rutz, J. M., Klebba, P. E., and Feix, J. B. (1994) *Biochemistry* **33**, 13274-13283

42. Ferguson, A. D., Chakraborty, R., Smith, B. S., Esser, L., van der Helm, D., and Deisenhofer, J. (2002) *Science* **295**, 1715-1719

43. Hashimoto-Gotoh, T., Franklin, F. C., Nordheim, A., and Timmis, K. N. (1981) *Gene* **16**, 227-235

44. Takeshita, S., Sato, M., Toba, M., Masahashi, W., and Hashimoto-Gotoh, T. (1987) *Gene* **61**, 63-74

45. Klebba, P. E., McIntosh, M. A., and Neilands, J. B. (1982) *J Bacteriol* **149**, 880-888

46. Rutz, J. M., Liu, J., Lyons, J. A., Goranson, J., Armstrong, S. K., McIntosh, M. A., Feix, J. B., and Klebba, P. E. (1992) *Science* **258**, 471-475

47. Teather, R. M., Bramhall, J., Riede, I., Wright, J. K., Furst, M., Aichele, G., Wilhelm, U., and Overath, P. (1980) *Eur J Biochem* **108**, 223-231

48. Yanisch-Perron, C., Vieira, J., and Messing, J. (1985) *Gene* **33**, 103-119

49. Annamalai, R., Jin, B., Cao, Z., Newton, S. M., and Klebba, P. E. (2004) *J Bacteriol* **186**, 3578-3589

50. Smallwood, C. R., Marco, A. G., Xiao, Q., Trinh, V., Newton, S. M., and Klebba, P. E. (2009) *Mol Microbiol* **72**, 1171-1180

51. Kaserer, W. A., Jiang, X., Xiao, Q., Scott, D. C., Bauler, M., Copeland, D., Newton, S. M., and Klebba, P. E. (2008) *J Bacteriol* **190**, 4001-4016

52. Neidhardt, F. C., Bloch, P. L., and Smith, D. F. (1974) *J Bacteriol* **119**, 736-747

53. Miller, J. H. (1972) *Experiments in molecular genetics*, Cold Spring Harbor Laboratory, Cold Spring Harbor, N.Y.

54. McIntosh, M. A., and Earhart, C. F. (1977) *J Bacteriol* **131**, 331-339

55. Sprencel, C., Cao, Z., Qi, Z., Scott, D. C., Montague, M. A., Ivanoff, N., Xu, J., Raymond, K. M., Newton, S. M., and Klebba, P. E. (2000) *J Bacteriol* **182**, 5359-5364

56. March, S. C., Parikh, I., and Cuatrecasas, P. (1974) *Anal Biochem* **60**, 149-152

57. Axen, R., Porath, J., and Ernback, S. (1967) *Nature* **214**, 1302-1304

58. Oudega, B., Oldenziel-Werner, W. J., Klaasen-Boor, P., Rezee, A., Glas, J., and de Graaf, F. K. (1979) *J Bacteriol* **138**, 7-16

59. Porath, J., Axen, R., and Ernback, S. (1967) *Nature* **215**, 1491-1492

60. Sims, P. J., Waggoner, A. S., Wang, C. H., and Hoffman, J. F. (1974) *Biochemistry* **13**, 3315-3330

61. Ames, G. F. (1974) *J Biol Chem* **249**, 634-644

62. Murphy, C. K., Kalve, V. I., and Klebba, P. E. (1990) *J Bacteriol* **172**, 2736-2746

63. McIntosh, M. A., and Earhart, C. F. (1976) *Biochem Biophys Res Commun* **70**, 315-322

64. Pugsley, A. P., and Reeves, P. (1976) *J Bacteriol* **126**, 1052-1062

65. Wayne, R., Frick, K., and Neilands, J. B. (1976) *J Bacteriol* **126**, 7-12

66. Davies, J. K., and Reeves, P. (1975) *J Bacteriol* **123**, 96-101

67. Benedetti, H., Lloubes, R., Lazdunski, C., and Letellier, L. (1992) *EMBO J* **11**, 441-447

68. Zakharov, S. D., Sharma, O., Zhalnina, M. V., and Cramer, W. A. (2008) *Biochemistry* **47**, 12802-12809

69. Yamashita, E., Zhalnina, M. V., Zakharov, S. D., Sharma, O., and Cramer, W. A. (2008) *EMBO J* **27**, 2171-2180

70. Saier, M. H., Jr. (2000) *J Membr Biol* **175**, 165-180

71. Gumbart, J., Wiener, M. C., and Tajkhorshid, E. (2007) *Biophys J* **93**, 496-504

72. Wang, C. C., and Newton, A. (1971) *J Biol Chem* **246**, 2147-2151

73. Guterman, S. K., and Dann, L. (1973) *J Bacteriol* **114**, 1225-1230

74. Reynolds, P. R., Mottur, G. P., and Bradbeer, C. (1980) *J Biol Chem* **255**, 4313-4319

75. Postle, K. (1993) *J Bioenerg Biomembr* **25**, 591-601

76. Pommier, S., Gavioli, M., Cascales, E., and Lloubes, R. (2005) *J Bacteriol* **187**, 7526-7534

77. Gerding, M. A., Ogata, Y., Pecora, N. D., Niki, H., and de Boer, P. A. (2007) *Mol Microbiol* **63**, 1008-1025

78. Wang, C. C., and Newton, A. (1969) *J Bacteriol* **98**, 1142-1150

79. Pugsley, A. P., and Reeves, P. (1977) *J Bacteriol* **130**, 26-36

80. Bradbeer, C. (1993) *J Bacteriol* **175**, 3146-3150

81. Goemaere, E. L., Cascales, E., and Lloubes, R. (2007) *J Mol Biol* **366**, 1424-1436

82. Nikaido, H., and Vaara, M. (1985) *Microbiol Rev* **49**, 1-32

83. Cascales, E., and Lloubes, R. (2004) *Mol Microbiol* **51**, 873-885

84. Pawelek, P. D., Croteau, N., Ng-Thow-Hing, C., Khursigara, C. M., Moiseeva, N., Allaire, M., and Coulton, J. W. (2006) *Science* **312**, 1399-1402

85. Shultis, D. D., Purdy, M. D., Banchs, C. N., and Wiener, M. C. (2006) *Science* **312**, 1396-1399

86. Bouveret, E., Benedetti, H., Rigal, A., Loret, E., and Lazdunski, C. (1999) *J Bacteriol* **181**, 6306-6311

87. Ferguson, A. D., Hofmann, E., Coulton, J. W., Diederichs, K., and Welte, W. (1998) *Science* **282**, 2215-2220

88. Locher, K. P., Rees, B., Koebnik, R., Mitschler, A., Moulinier, L., Rosenbusch, J. P., and Moras, D. (1998) *Cell* **95**, 771-778

89. Buchanan, S. K., Lukacik, P., Grizot, S., Ghirlando, R., Ali, M. M., Barnard, T. J., Jakes, K. S., Kienker, P. K., and Esser, L. (2007) *EMBO J* **26**, 2594-2604

90. Novo, D., Perlmutter, N. G., Hunt, R. H., and Shapiro, H. M. (1999) *Cytometry* **35**, 55-63

91. Suzuki, H., Wang, Z. Y., Yamakoshi, M., Kobayashi, M., and Nozawa, T. (2003) *Analytical sciences : the international journal of the Japan Society for Analytical Chemistry* **19**, 1239-1242

92. Kadner, R. J., and McElhaney, G. (1978) *J Bacteriol* **134**, 1020-1029

93. Gutfreund, H. (1995) *Kinetics for the life sciences : receptors, transmitters, and catalysts*, Cambridge University Press, Cambridge ; New York

94. Jiang, X., Payne, M. A., Cao, Z., Foster, S. B., Feix, J. B., Newton, S. M., and Klebba, P. E. (1997) *Science* **276**, 1261-1264

95. Nikaido, H., and Rosenberg, E. Y. (1981) *J Gen Physiol* **77**, 121-135

96. Cowan, S. W., Garavito, R. M., Jansonius, J. N., Jenkins, J. A., Karlsson, R., Konig, N., Pai, E. F., Pauptit, R. A., Rizkallah, P. J., Rosenbusch, J. P., and et al. (1995) *Structure* **3**, 1041-1050

97. Luria, S. E. (1964) *Ann Institute Pasteur (Paris)* **107**, (Suppl.): 67–73.

98. Chu, B. C., Peacock, R. S., and Vogel, H. J. (2007) *Biometals* **20**, 467-483

99. Postle, K., and Kadner, R. J. (2003) *Mol Microbiol* **49**, 869-882

100. Pramanik, A., Zhang, F., Schwarz, H., Schreiber, F., and Braun, V. (2010) *Biochemistry* **49**, 8721-8728

101. Pramanik, A., Hauf, W., Hoffmann, J., Cernescu, M., Brutschy, B., and Braun, V. (2011) *Biochemistry* **50**, 8950-8956

102. Higgs, P. I., Larsen, R. A., and Postle, K. (2002) *Mol Microbiol* **44**, 271-281

103. Ollis, A. A., Manning, M., Held, K. G., and Postle, K. (2009) *Mol Microbiol* **73**, 466-481

104. Newton, S. M., Trinh, V., Pi, H., and Klebba, P. E. (2010) *J Biol Chem* **285**, 17488-17497

105. Hahn, M. W., and Hofle, M. G. (1999) *Appl Environ Microbiol* **65**, 4863-4872

106. Wang, J., Galgoci, A., Kodali, S., Herath, K. B., Jayasuriya, H., Dorso, K., Vicente, F., Gonzalez, A., Cully, D., Bramhill, D., and Singh, S. (2003) *J Biol Chem* **278**, 44424-44428